Robust multi-objective design of suspension systems

Muhammad Ali Khan
khan75@marshall.edu

ROBUST MULTI-OBJECTIVE DESIGN OF SUSPENSION SYSTEMS

A thesis submitted to
the Graduate College of
Marshall University
In partial fulfillment of
the requirements for the degree of
Master of Science
In
Mechanical Engineering
by
Muhammad Ali Khan
Approved by
Dr. Yousef Sardahi,
Dr. Gang Chen,
Dr. Asad Salem

Marshall University
December 2020

APPROVAL OF THESIS

We, the faculty supervising the work of **Muhammad Ali Khan**, affirm that the thesis titled "**ROBUST MULTI-OBJECTIVE DESIGN OF SUSPENSION SYSTEMS**", meets the high academic standards for original scholarship and creative work established by the Master of Science in Mechanical Engineering and the College of Information Technology and Engineering. This work also conforms to the editorial standards of our discipline and the Graduate College of Marshall University. With our signatures, we approve the manuscript for publication.

Dr. Yousef Sardahi	Committee Chairperson	Date 11-20-2020
Dr. Gang Chen,	Committee Member	Date 11/20/2020
Dr. Asad Salem	Committee Member	Date 11-20-2020

ACKNOWLEDGMENTS

To supervisor, Dr. Yousef Sardahi, thank you for your assistance and guidance throughout this research. To the committee members, Dr. Asad Salem and Dr. Gang Chen, thank you for your inputs and reviewing my work. To my family, thank you a lot for your support and motivation throughout this degree.

TABLE OF CONTENTS

LIST OF FIGURES

ABSTRACT

This thesis presents a robust multi-objective optimal design of four-degree-of-freedom passive and semi-active suspension systems. The passive suspension system is used in a racing car and the semi-active suspension is implemented on a passenger car. Mathematical models of the commercial and racing vehicle suspension systems are used in the computer simulations. A robust multi-objective design of the suspension systems is carried out by considering the minimization of three objectives: passenger's head acceleration (HA), suspension deflection (SD), and tire deflection (TD). The first objective is concerned with the passenger's health and comfort. The suspension stroke is described by SD and the tire holding is characterized by TD. The optimal design of the passive suspension involves tuning the coefficients of the sprung spring and damper, tire stiffness, and inertance of the inerter. Suspension systems' parametric variations are very common and cannot be avoided in practice. To this end, a robust multi-objective optimization method that takes into consideration small changes in the design parameters should be considered. Unlike traditional multi-objective optimization problems where the focus is placed on finding the global Pareto-optimal solutions which express the optimal trade-offs among design objectives, the robust multi-objective optimization algorithms are concerned with robust solutions that are less sensitive to perturbations of decision variables. As a result, the mean effective values of the fitness functions are used as design objectives. Constraints on the design parameters and goals are applied. Numerical simulations show that the robust multi-objective design (RMOD) is very effective and guarantees a robust behavior as compared to that of the classical multi-objective design (MOD). The results also show that the robust region is inside the feasible search space and avoids all of its boundaries. The decision

parameter space of the semi-active suspension includes both passive and active components. The passive components include the stiffness of the sprung spring, damping coefficient of the shock absorber, and stiffness of the tire. The active elements are the design details of the LQR algorithm. During the design, global sensitivity analysis is conducted to determine the elements of the suspension system that have high impact on the design objectives. The mass of the passenger's head and upper body, the mass of the passenger's lower body and cushion, passenger and cushion's elastic properties, and the sprung mass of the vehicle are selected for the sensitivity analysis. Results show that the design goals are more sensitive to the variations in the sprung mass than the other parameters. As a result, parametric variations in the sprung mass of the vehicle and passive elements of the suspension system are considered. Similar to the design of the passive suspension, the mean effective values of SD, TD, and HA are used as design objectives. Also, constraints are applied on the objectives in compliance with the requirements of ISO 2631-1 on the design of car suspension systems. The optimization problem is solved by the NSGA-II (non-dominated sorting genetic algorithm) and robust Pareto front and set are obtained.

CHAPTER 1: INTRODUCTION

1.1 Literature Review

Most of the real-world design problems have complex multidisciplinary objectives. For example, in the optimal design of the suspension system, the most common design targets are the comfort, road handling, and suspension stability. Furthermore, the multi-objective design technique is employed to obtain a Pareto-optimal solution set, which gives the designer the real picture of the problem before making the final selection. Vehicle suspension systems, in terms of their multi contradictory objectives, have been widely studied over the last three decades (Callejo, Jalon, Luq, & Mantaras, 2015). The role of a vehicle suspension system is to provide road comfort to the occupants and assurance of handling stability. Overall, the vehicle suspension systems can be put into three categories: active suspension system, semi-active suspension system, and passive suspension system. Passive suspension systems are widely used because of their high dependability, no energy consumption, simplicity, and they are comparatively less expensive than active and semi-active suspension systems. They consist of only passive elements such as springs, masses, dampers, and inerters. However, active and semi-active suspension systems comprise of controllable suspension system equipped with sensors and electronic control units.

Several studies have been focused on the optimal design of passive suspension systems. For instance, Alfonso and his colleagues investigated a multi-objective optimal design of a multi-body suspension system by considering two objectives: passengers' comfort and road handling (Callejo et al., 2015). The front and rear dampers, rear air springs, front air springs, body work stiffness, rear antiroll bar, rear relaxed length, front relaxed length, and bodywork stiffness are chosen as setup parameters. Two optimization constraints were defined to specify the commercial vehicle safety which include the lateral contact force and the tire grip. After that, the sensitivity analysis was conducted by C++ and MATLAB. The results showed that the multi-objective approach is beneficial in obtaining optimal trade-offs among the design targets.

In the second study (Xu, Sardahi, & Zheng, 2018), a passive suspension system with inerter was presented. Four design objectives were considered: suspension deflection, crest factor, occupant’s head acceleration, and tire deflection. The multi-objective optimization problem was solved by the non-dominating sorting genetic algorithm (NSGA-II) to obtain the trade-offs among the design objectives. The spring stiffness and damper, spring constant of the tire, and the inertance were selected as design variables. Upper and lower bounds were imposed on these parameters. The results showed competing relationships between the design targets and the necessity to handle the design problem in multi-objective settings.

In the third study, an analytical approach was proposed to solve the multi-objective optimization problem of a passive suspension system. A half car model was used in the analysis to quantify three design objectives: reduction of the root mean square values in the cushion acceleration, improving the tire grip, and enhancing the suspension deflection (Bhargav Gadhvi, 2016). The optimization problem was solved using three multi-objective evolutionary algorithms (MOEAs): NSGA-II, SPEA-II (Strength Pareto Evolutionary Algorithm II), and PESA-II (Pareto Envelope-Based Selection Algorithm II). Constraints on the seat acceleration, tire deflection, and suspension deflection were imposed. The front tire deflection and rear tire deflection were selected as design parameters. The results showed that Pareto front obtained from NSGA-II provides a better optimal solution for the optimization problem compared to the other algorithms.

A robust multi-objective optimal (RMOP) design of an uncertain passive suspension of a quarter car was conducted (Loyer & Jézéquel, 2009). The road holding and ride comfort were considered as design objectives. The stiffness of the spring and the damper of the shock absorber connected to the sprung mass were selected as design parameters. Two constraints on the wheel travel, and body bounce mode natural frequency were imposed. The spring mass and tire stiffness were considered uncertain and the optimization problem was solved by a multi-objective evolutionary algorithm (MOEA). The result obtained by the algorithm gives the designer clear image of the suspension tuning possibilities by subjecting the desired variants, objective robustness, and the product line.

A five-degree-of-freedom model with a passive suspension system was designed in multi-objective settings using a multi-objective uniform diversity genetic algorithm (Nariman-Zadeh, Salehpour, Jamali, & Haghgoo, 2010). The seat acceleration, rear tire velocity, forward tire velocity, and suspension travel of the front and rear tire are selected as design targets. These conflicting design targets are evaluated by adjusting the seat mass; rear tire mass; momentum inertia of the sprung mass; forward tire stiffness coefficient; rear tire stiffness constant; sprung mass; forward and rear tires' positions; and forward tire mass. The equality constraints were applied during the optimization. The results showed that there are many optimal solutions that the decision-maker can choose from to implement.

A vector optimization of a passive suspension parameters was achieved by using evolutionary computation (Goga & Kľúčik, 2012). The optimization performed was based on advancing the occupant's comfort and driving stability. The optimization objectives considered were to reduce the vertical acceleration, minimizing the angular acceleration, and lowering the vertical displacement. The stiffness coefficients and damping coefficients were considered as optimized design parameters. The results obtained by using MATLAB Simulink indicated that the driving stability and occupant's comfort was not as satisfying for the passive suspension system as compared to the other vehicle suspension system.

In another study, a multi-objective optimization (MOP) of a passive suspension system for a full car model was conducted to obtain global optimal Pareto solutions (Fossati, Miguel, & Casas, 2019). The passenger comfort, tire grip, and suspension travel were the conflicting objectives that were selected in this optimization problem. These conflicting objectives were evaluated by six design parameters which include driver seat stiffness coefficient, front spring stiffness coefficient, rear spring stiffness coefficient, driver seat damping coefficient, front dampers damping coefficient, and rear dampers damping coefficient. The NSGA-II was employed to obtain the three-dimensional Pareto optimal solution. The result indicated that the proposed methodology is an effective tool for the optimal design of passive suspension systems in terms of passenger ride comfort and stability.

A multi-objective optimization of the performance of a passive vehicle model was achieved by considering the road excitation (Jamali, Shams, & Fasihozaman, 2014). The acceleration of the seat, working space, and vertical tire velocity were used as design targets. The seat stiffness coefficient, suspension stiffness coefficient, seat damping coefficient, suspension damping coefficient, and seat position were presented as design variables. The system is solved by a multi-objective uniform diversity algorithm to obtain global Pareto optimal solutions and system frequency response. The optimization results indicated that the proposed methodology allows the designer to select the ultimate design to achieve the desired performance criteria.

Another optimal design of a passive suspension system for a military vehicle was presented (Mahmoud Mohsen, 2018). The driver body vertical displacement, seat vertical displacement, and seat suspension working space were considered as fitness functions. The stiffness and damping coefficients of the suspension system, driver seat suspension, and seat cushion were chosen as design parameters. The genetic algorithm was employed to optimally adjust the decision variables and minimize the design objectives simultaneously. The results manifested an improvement in the dynamic performance of vehicle suspension system.

Similarly, an optimal design of a passive car suspension system was performed by multi-objective evolutionary algorithms (Niahn-Chung Shieha, 2004). The objective goal was to find the optimal compromise between ride quality and sprung mass suspension stroke. Eight tuning parameters related to the suspension spring stiffness and damping coefficient were selected and their feasible constraints were defined. The results showed that ride quality is improved by expanding the working space of the car suspension system.

Several studies have been reported about the multi-objective optimal design of semi-active suspension systems. For example, a multi-objective design of a semi-active car suspension system with magnetorheological dampers was performed (Crews, Mattson, & Bucker, 2011). Two conflicting objective functions are selected which include the thermal performance and absorbed power. The control limitations are implemented on the control inputs which are taken as design variables. Skyhook, feedback linearization, and sliding mode controls are implemented and their performances are compared. The optimization is performed by a multi-objective genetic algorithm to achieve the final Pareto frontier. The results showed that this approach was not able to accommodate real-time control solutions that would operate with the Pareto frontier.

A semi-active suspension system with a magnetorheological suspension system was evaluated in wheel electric vehicles (Anaya-Martinez, et al., 2020). The main goal was to achieve a compromise solution between better road grip and ride comfortability. A switched reluctance motor was attached to the unsprung mass for engaging the spring and dampers to achieve a vibration reduction. The simulation results obtained from pseudo bode plots showed that the skyhook and Mix one sensor controller provide the best enhancement in terms of the design goals.

In another work, an optimal design of a semi-active suspension system is conducted by genetic algorithms (Koulocheris, Papaioannou, & Chrysos, 2017). The root-mean-square acceleration and the median of front and rear wheel travel were determined as cost functions. The damping coefficient of the suspension system and spring stiffness of the tire were defined in the working space. The skyhook two-state damper control, skyhook linear approximation damper control, power-driven damper control, acceleration driven damper control, and mixed skyhook acceleration driving control were used as control algorithms. The study provided detailed comparisons among these techniques.

A continuous skyhook control and modified skyhook control were employed in the optimal control of a semi-active suspension system in two-wheeled vehicles (Khadr & Romdhane, 2016).The root-mean-square of vertical acceleration of the chassis and the wheel dynamic load were selected as design targets to achieve the best comfort and the drive safety. The front and rear damping coefficients of skyhook dampers were defined as design parameters. The NSGA-II was used to solve the optimization problem. The multi-objective optimization results exhibited that both control laws guarantee the highest comfort and dive safety.

A linear quadratic regulator (LQR) and mixed H_2/H_∞ optimization control was employed in the optimal design of a semi-active suspension system (Ye & Zheng, 2019). The vehicle vertical acceleration, suspension travel, and wheel dynamic load were defined as control objectives. Numerical simulations were carried out by MATLAB/Simulink and compared with those of the passive suspension system. The performance of the closed-loop system under these control strategies showed improved comfort and road handling.

Fuzzy and PID controls were developed for a semi-active suspension system with magnetorheological damper (Lazaro, Villegas, Ruiz, & Aldana, 2019). Passengers' comfort, ride handling, and ground contact of the wheel were selected as control objectives. The results demonstrated that both control strategies were proven to be effective, but the fuzzy controller was the most acceptable in terms of comfortability.

A Model predictive control (MPC) algorithm for vibration attenuation was applied on a semi-active suspension system with a magnetorheological (MR) damper (Mai, Yoon, Choi, & Kim, 2020). The vertical sprung mass acceleration and sprung mass displacement were defined as design objectives. Both bump and random excitations were used as inputs to test the performance of the controlled system numerically and experimentally. The results demonstrated that the algorithm successfully achieved the highest ride comfort and road handling for the semi-active suspension system with MR dampers.

An adaptive optimal controller with policy iteration algorithm for a semi active suspension system with MR damper was presented by Wang (Xiaolong, 2017). The acceleration of sprung mass, sprung mass travel, tire deflection, and suspension deviation were chosen as design criteria for bump excitation response. The responses of the system under the adaptive control algorithm were compared with those of linear quadratic regulator algorithm assuming the system is excited by a step input. The simulation results showed that the adaptive optimal controller outperforms the linear quadratic regulator method.

An optimal control design of a semi-active suspension system consisting of a magnetorheological shock absorber under both skyhook and linear quadratic regulators was presented (Majdoub et al., 2018). The chassis vertical travel and drive comfort were used as cost functions. The viscous damping coefficients and wheel stiffnesses were defined as design parameters. The numerical simulations obtained by MATLAB/Simulink manifested that the performance of the suspension system under the linear quadratic regulator was better than that of the skyhook controller.

A Commande Robuste Ordre Non-Entier (CRONE) - Skyhook control approach was proposed (Frej, Moreau, Hamrouni, Benine-Neto, & Hernette, 2020) for a passenger-sport car with a multi-mode semi-active suspension system. The control criteria were to achieve the best solution between minimum frequency convenience and controlled chassis movement. The vertical stiffness of the wheel, stiffness coefficient of the suspension, damping coefficient of the tire, and damping of the suspension were taken as design variables. The control criteria were analyzed through the CRONE-Skyhook control approach and mode shifting was performed. The results showed that the car stability and occupant's comfort were achieved.

Multi-objective optimization control for semi active suspension system in self-driving car is proposed in view of car speed and suspension vibration (Wu, Zhou, Liu, & Gu, 2020). The optimization goal was to achieve the best car comfort performance and maximum suspension adaptability to four different speed trajectories. The hybrid horizon varying (HV) model predictive control (MPC) approach is employed as a suspension controller to adjust the upright and longitudinal acceleration making use of random road excitation information. The simulation results demonstrated the efficacy of the HV-MPC control approach and the importance of designing the suspension system by considering more than one objective.

Energy efficient look-ahead cruise controller integrated with adaptive semi-active suspension system was presented for a utility commercial vehicle (Basargan, Mihάly, Gáspár , &

Sename, 2020). The optimization criteria were to minimize the horizontal control force and the velocity limits for achieving the occupant's comfort and ride stability. The tire stiffness, damping rate of the shock absorber and spring stiffness were defined as design variables. The multi-criteria optimization problem was solved by the look-ahead estimation algorithm based on global positioning system. The results showed an improved vehicle adaptability based on the variations of the vehicle velocity.

Based on the above literature review, the significance of uncertainties in the mechanical components such as spring, damper, and inerter for the passive suspension system was not considered. The passive components of the suspension system are uncertain due to either manufacturing errors, or operation. Their values will certainly impact the performance of the suspension system. Robust multi-objective optimization technique is proposed to fill the above research gap in the literature. The robust multi-objective optimization method aims to reduce the sensitivity of the design objectives to the uncertainties in the design parameters. The solution of the robust multi-objective optimization problem is expected to be less sensitive to parametric variations as compared to that of the traditional multi-objective optimization.

In the next sections, we introduce the concepts of classical and robust multi-objective optimization, delineate the working principle of NSGA-II, and outline of the thesis.

1.2 Multi-Objective Optimization

Multi-objective optimization problems (MOPs) have received much attention recently because of their enormous applications. A MOP can be stated as follows:

$$\min_{k \in D}\{\mathbf{F}(\mathbf{k})\}, \tag{1}$$

where **F** is the map that consists of the objective functions f_i: Q → R^1 under consideration.

$$\mathbf{F}: Q \rightarrow \mathbf{R}^{k}, \mathbf{F}(\mathbf{k}) = [f_1(\boldsymbol{k}),\ \dots,\ f_k(\boldsymbol{k})]. \tag{2}$$

$\mathbf{K} \in \boldsymbol{D}$ is a q-dimensional vector of design parameters. The domain $D \subset \mathbf{R}^{\boldsymbol{q}}$ can in general be expressed by inequality and equality constraints:

$$D = \{\mathbf{k} \in \mathbf{R}^{\boldsymbol{q}} | \; g_i(\mathbf{k}) \leq 0, i = 1, \dots, l, and \;\; h_j(\mathbf{k}) = 0, j = 1, \dots, m \}. \qquad (3)$$

Where there are *l* inequality and *m* equality constraints. The solution of MOPs forms a set known as the Pareto set and the corresponding set of the objective values is called the Pareto front. The dominancy concept (Marler & Arora, 2004) is used to find the optimal solution. The MOPs are solved using multi-objective optimization algorithms. These methods can be classified into scalarization, Pareto, and non-scalarization non-Pareto methods (Sardahi, 2016).

The scalarization methods such as the weighted sum, goal attainment, and lexicographic approach require transformation of the MOP into a single optimization problem (SOP) (Pareto, 1971), normally by using coefficients, exponents, constraint limits, etc.; and then methods for single objective optimization are utilized to search for a single solution. Computationally, these methods find a unique solution efficiently and converge quickly. However, these methods cannot discover the global Pareto solution for non-convex problems. Also, it is not always clear for the designer to know how to choose the weighting factors for the scalarization (Hernández et al., 2013).

Unlike the scalarization methods, the Pareto methods do not aggregate the elements of the objectives into a single fitness function. They keep the objectives separate all the time during the optimization process. Therefore, they can handle all conflicting design criteria independently, and compromise them simultaneously. The Pareto methods provide decision-makers with a set of solutions such that every solution in the set expresses a different trade-off among the functions in the objective space. Then, the decision-maker can select any point from this set. Compared to the scalarization approaches, the Pareto methods can successfully find the optimal or near optimal solution set, but they are computationally more expensive. Examples of algorithms that fall under this category are the MOGA (Multiple Objective Genetic Algorithm), PSO (Particle Swarm Optimization), NSGA-II (Non-dominated Sorting Genetic Algorithm), SPEA2 (Strength Pareto Evolutionary Algorithm), and NPGA-II (Niched Pareto Genetic Algorithm). Mainstream evolutionary algorithms for MOPs include NSGA-II, multi-objective particle swarm optimization (MOPSO) and strength Pareto evolutionary algorithm (SPEA). Deterministic methods such as set oriented methods with subdivision techniques, and multi-objective algorithms based on the simple cell mapping (SCM) can be also used to find the solution set (Sardahi, 2016).

The $\epsilon-$constraint method and the VEGA (Vector Evaluated Genetic Algorithm) approach are examples of the non-scalarization non-Pareto methods. In the $\epsilon-$constraint method, one of the cost functions is selected to be optimized and the rest of the functions in the objective space are converted into constraints by setting an upper bound to each of them. The VEGA works almost in the same way as the single objective genetic algorithm, but with a modified selection process. A comprehensive survey of the methods used for solving MOPs can be found in (Jones, Mirrazavi, & Tamiz, 2002), (Marler & Arora, 2004), and (Tian, Cheng, Zhang, & Jin, 2017).

Passive and semi-active suspension systems can be optimally designed by using any one of these techniques. The optimization problems of these systems are complex and nonconvex, therefore evolutionary algorithms are methods of choice (Woźniak, 2010). They outperform classical direct and gradient based methods which suffer from the following problems when dealing with non-linear, non-convex, and complex problems: 1) the convergence to an optimal solution depends on the initial solution supplied by the user, and 2) most algorithms tend to get stuck at a local or sub-optimal solution. On the other side, evolutionary algorithms are computationally expensive (Hu, Huang, & Wang, 2003). However, this cost can be justified if a more accurate solution is desired and the optimization is conducted offline. The most widely used multi-objective optimization algorithm is the NSGA-II (Sardahi & Boker, 2018) and (Xu et al., 2018). It yields a better Pareto front as compared to other algorithms (Gadhvi, Savsani, & Patel, 2016). Therefore, in this paper, we use the NSGA-II to solve the robust multi-objective problems.

1.3 Robust Multi-Objective Optimization

Robust optimization has considerable advantage over traditional Multi-objective optimization (MOP). Traditional multi-objective optimization problems seek to find global Pareto solutions without considering uncertainties in the system parameters. On the other side, robust multi-objective approaches seek to find the less sensitive trade-offs among the design goals. A Robust Multi-objective optimization problem (RMOP) can be stated as follows:

$$\min_{\mathbf{K}\in\mathbf{Q}}\{\,\mathbf{F}^{\mathbf{eff}}\,(\mathbf{k})\} \tag{4}$$

where $\boldsymbol{F}^{eff}$ is the map that consists of the mean effective objective functions f_i^{eff} : Q→R^1 under consideration.

$$\boldsymbol{F}^{eff}: Q \to R^k, F^{eff}\,(\boldsymbol{k}) = \left[f_1^{eff}(\boldsymbol{k}), \dots\dots, f_k^{eff}\,(\boldsymbol{k})\right] \tag{5}$$

$\mathbf{k}$ ∈ Q is a q-dimensional vector of design parameters. The domain Q⊂ $\mathbb{R}^q$ can in general be expressed by mean effective inequality and equality constraints:

$$Q = \{k \in \mathbb{R}^q \mid g_i^{eff}(k) \le 0, i = 1, \dots\dots., l, \tag{6}$$

$$and\ h_j^{eff}\,(k) = 0, j = 1, \dots.., n\}.$$

Where, fi^{eff} is defined as:

$$f_i^{eff} = \frac{1}{|\mathbf{B}_{\boldsymbol{\delta}}(\mathbf{k})|} \int_{\mathbf{y} \in \mathbf{B}_{\boldsymbol{\delta}}(\mathbf{k})} f_i(\boldsymbol{y}) d\boldsymbol{y}. \tag{7}$$

Where $\boldsymbol{\delta}$ is a q-dimensional vector of parameters' uncertainties is the-neighborhood of the solution $\mathbf{B}_{\delta}(\mathbf{k})$ is the δ-neighborhood of the solution $\mathbf{k}$ (k is perturbed in the neighborhood $[\mathbf{k}-\boldsymbol{\delta},\mathbf{k}+\boldsymbol{\delta}]$ and $|\mathbf{B}_{\delta}(\mathbf{k})|$ is the hyper-volume of the neighborhood. To use this definition in practice, a finite set of H solutions can be randomly generated within the perturbed range of $\mathbf{k}$ and then used to evaluate $\boldsymbol{F}^{eff}$ (Deb & Gupta, Introducing robustness in multi-objective optimization, 2006).

1.4 Evolutionary algorithm

The genetic algorithm is used to solve a multi-objective optimization problem to obtain a Pareto optimal front. The algorithm used in this research is the non-dominating genetic algorithm. The algorithm begins with population initialization with the consideration of constraints. The initialization set contains all the individual elements of objective functions that are dominated by population P. The algorithm is best with comparison to the older version because the information of define set dominates the individual. Further, the population is defined as the crowding distance is assigned, where the distance between each individual is calculated based on their multi-objectives. After the distance is allocated the selection is performed using the comparison operator. These individuals are selected by tournament selection with a comparison operator to influence the objective. The genetic operator for crossover and mutation is initialized to obtain the sample distribution of generated values between zero and one. The successor population is combined with the current population to achieve the best upcoming generation.

The control parameters of the genetic algorithm are adjusted to obtain the best performance. The parameter included the probability of crossover, distribution index, mutation probability, and pollution size. These define control parameters provide with best convergence and dispersion of the Pareto optimal points located on the Pareto front. The flow chart of the genetic algorithm is shown in Figure 1 (Kanagarajan, Karthikeyan, Palanikumar, & Paulo Davim, 2008).

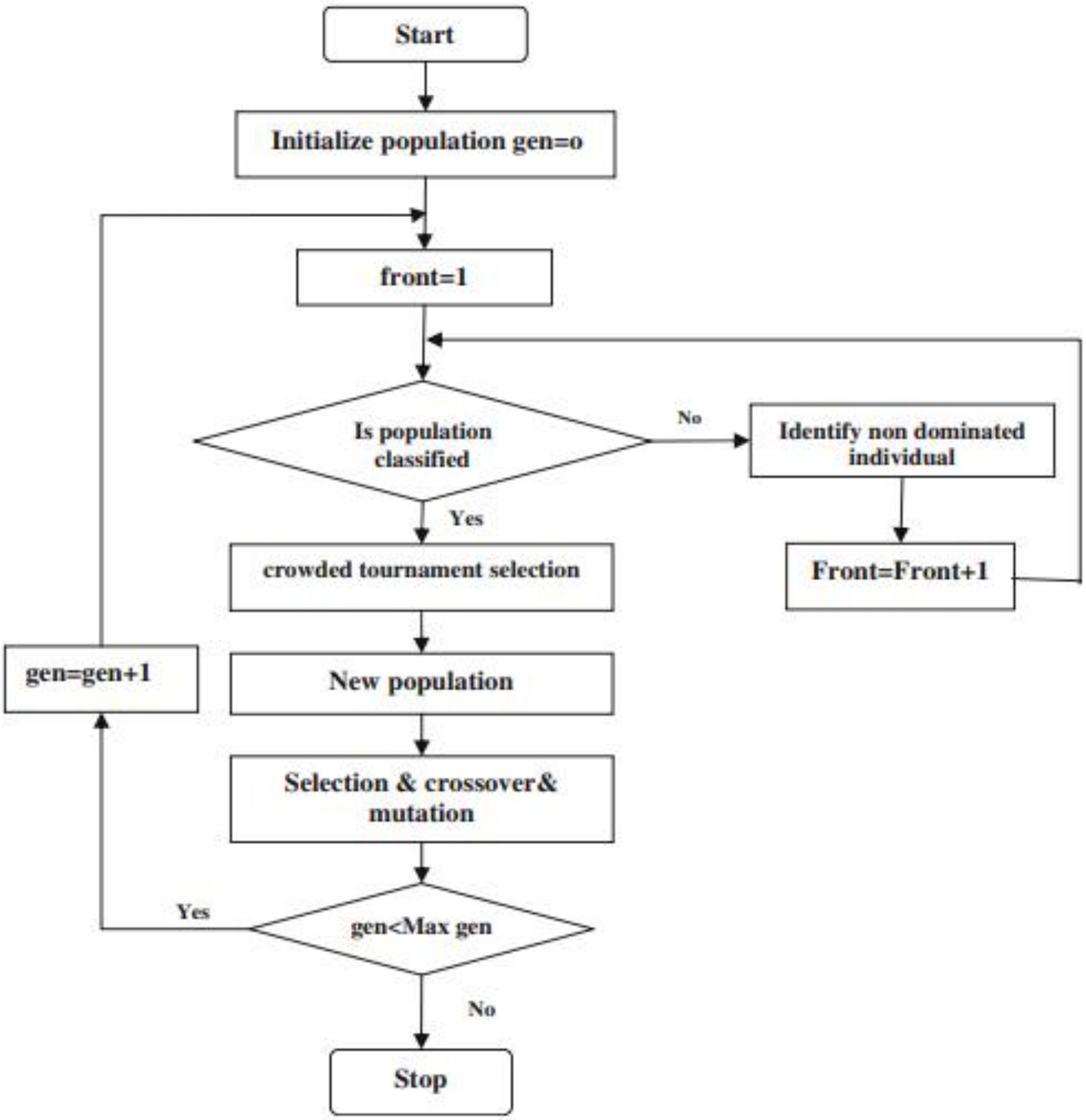

***Figure 1**: The flow chart of genetic algorithm.*

1.5 Outline of the Thesis

This thesis is based on the research and publications on the robust multi-objective optimal design of suspension systems. Chapter 1 describes the introduction. Chapter 2 presents the robust multi-objective optimal design of a racing car suspension system. Chapter 3 proposes a multi-objective and robust design of a semi-active suspension system of a passenger car. Chapter 4 summarizes the thesis and suggests future directions.

CHAPTER 2: ROBUST MULTI-OBJECTIVE OPTIMAL DESIGN OF A RACING CAR SUSPENSION SYSTEM

2.1 Introduction

The role of a vehicle suspension system is to provide road comfort to the occupants, and guarantee stability and road handling. In general, vehicle suspension systems can be classified as active, semi-active, and passive suspension systems. Active suspension systems were last seen in racing cars such as Formula 1 (F1) in 1993. Recently, F1 rejected a proposal to permit active suspensions in 2021 (Keith, 2019). Passive suspension has been widely used in racing cars due to their high reliability, simplicity, and low cost compared to the other types. Conventional passive schemes are based around two components - springs and shock absorbers (dampers). A new device called inerter was introduced in 2002 with the motivation to improve the mechanical grip of racing cars. Studies have also shown that inerters can significantly improve ride comfort, tire grip, and handling in comparison to standard passive systems (Papageorgiou, Houghton, & Smith, 2009)**.**

This chapter presents a robust multi-objective optimal design of a racing car suspension system. Three design objectives are considered: passenger's head acceleration, suspension travel, and tire deflection. The first objective is concerned with the passenger's health and comfort, second requirement characterizes the suspension stroke, and the third criterion describes the tire grip. To quantify the design objectives, the vertical dynamics of a quarter-car model employing an inerter is considered. The coefficients of the sprung spring and damping, tire stiffness, and inertance of the inerter are chosen as decision variables. The effect of design parameters' variations on the optimal solution is also considered. To this end, a robust multi-objective optimization problem is formulated and solved by the Non-dominated Sorting Genetic Algorithm

(NSGA-II). Unlike traditional multi-objective optimization problems where the focus is placed on finding the global Pareto-optimal solutions which express the optimal trade-offs among design objectives, the robust multi-objective optimization methods are concerned with robust solutions that are less sensitive to decision variables' perturbations. As a result, the mean effective values of the fitness functions are used as design objectives. Constraints on the design parameters and goals are applied. Numerical simulations are conducted on a quarter car model of a racing car. Details about this model are introduced in the next section.

2.2 Racing Car Suspension System Mathematical Model

The concept of "inerter" was first proposed in 2002 by Smith (Smith, 2002). Inerters are the mechanical equivalents of ungrounded capacitors, using the force–current analogy between mechanical and electrical circuits. In the industry sector, inerter is known as J-damper. Soon after it was introduced, the J-damper was implemented in the suspension systems of Formula 1 racing cars. McLaren Mercedes started using the J-damper in early 2005. In the same year, Kimi Raikkonen was the first one to race with a McLaren MP4- 20 having the inerter as a part of its suspension system at the 2005 Spanish Grand Prix and he won the competition. Inerters also have found their applications (Perlikowski, 2017) in the suspension systems of railway vehicles (Wang, Hsieh, & Chen, 2012), (Jiang, Matamoros-Sanchez, Goodall, & Smith, 2012), (Jiang, Matamoros-Sanchez, Zolotas, Goodall, & Smith, 2015), devices that absorb impact forces (Faraj, Holnicki-Szulc, Knap, & Seńko, 2016) or protect buildings from earthquakes (Takewaki, Murakami, Yoshitomi, & Tsuji, 2012), (Chen, Tu, & Wang, 2015) and steering compensators for motorcycles (Evangelou, Limebeer, Sharp, & Smith, 2007).

Inerters alleviate mechanical loads on the suspension and improve its handling and gripping performance (Chen, Papageorgiou, Scheibe, & Wan, 2009). The fact that adding an inerter device into the suspension structure can decrease the natural frequencies of the system was proved algebraically (Chen, Hu, Huang, & Chen, 2014). Schematically, the inerter element is a one port (two-terminal) mechanical network as shown in Figure 2 (Smith, 2002)**.** A linear inerter can be constructed by meshing a nut, screw, bearing, gear and flywheel which rotates in proportion to the relative displacement between the terminals. The screw forms one terminal of the device and the other terminal is mounted on the casing that houses the gears. The applied force induces relative acceleration on both terminals which is further transmitted into rotational motion of the flywheel using gear and pinion assembly. The dynamic equation of the inerter element reads

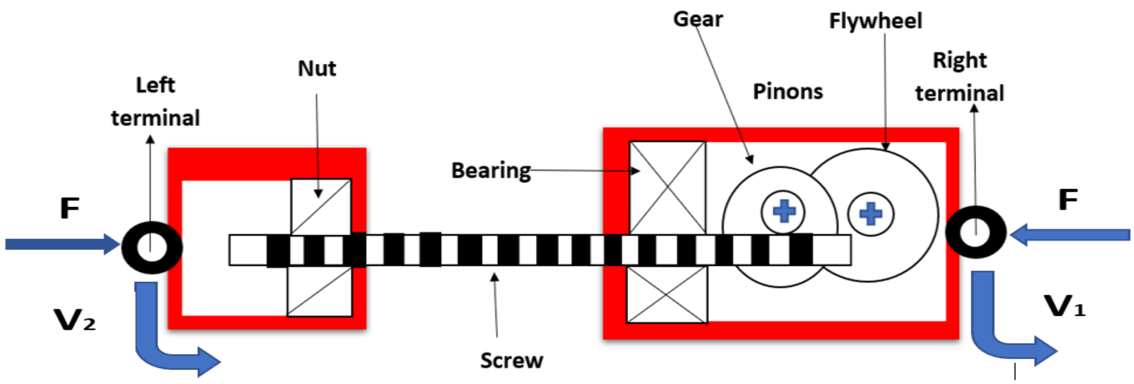

Figure 2: *A one-port (two-terminal) mechanical element.*

$$F = B\,(v_2 - v_1), \tag{8}$$

where, F is the force at the two terminals of the inerter, B is the inertance of the inerter in kg, and v_1 and v_2 are denote velocities of the two terminals of the inerter. A four-degree-of-freedom quarter car model implementing inerter in its suspension part is depicted in Figure 3 and its dynamic equations read

$$m_t\ddot{z}_t = -c_t(\dot{z}_t - \dot{z}_p) - k_t(z_t - z_p) \tag{9}$$

$$m_p\ddot{z}_p = c_t(\dot{z}_t - \dot{z}_p) + k_t\,(z_t - z_p) - c_c\,(\dot{z}_p\text{-}\dot{z}_s) - k_c(z_p - z_s), \tag{10}$$

$$m_s\ddot{z}_s = c_c(\dot{z}_p - \dot{z}_s)\dot{z}_p + k_c(z_p - z_s) - c_s(\dot{z}_s - \dot{z}_u) - k_s(z_s - z_u) - B(\ddot{z}_s - \ddot{z}_u) \tag{11}$$

$$m_u\ddot{z}_u = c_s(\dot{z}_s - \dot{z}_u) + k_s(z_s - z_u) - k_y(z_u - z_y) + B(\ddot{z}_s - \ddot{z}_u) \tag{12}$$

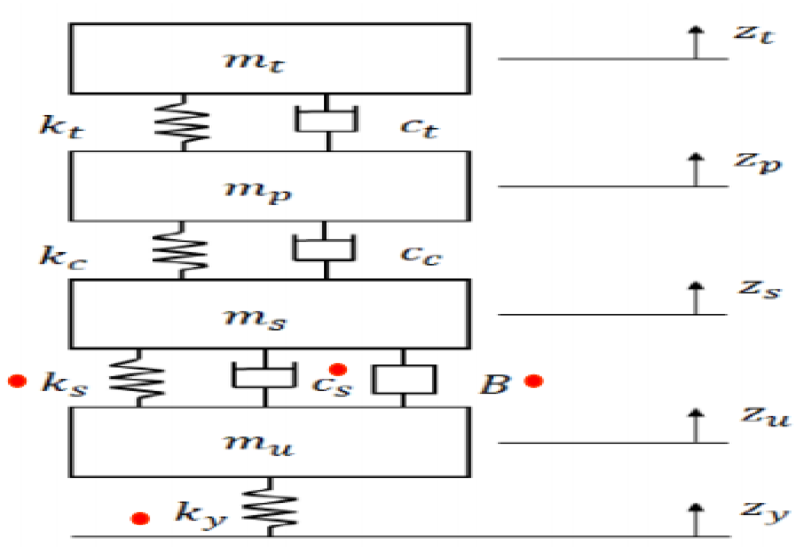

Figure 3: *The quarter car model of passive suspension system with inerter (Xu, Sardahi, & Zheng, 2018)*

Among them, m_t and m_p are respectively the equivalent mass of head and upper body, and lower body and cushion. That is, the passenger is modelled as a two-degree-of-freedom system by splitting the passenger's body mass into two parts: m_t and m_p such that m_p is connected to m_t by an assumed spring k_t and damper c_t. The cushion's elastic properties are modeled as an equivalent spring k_c and damper c_c which couple m_p to the sprung mass m_s. The suspension system is modeled as a spring with constant k_s, damper with coefficients, and an inerter having B as its constant. The tunable parameters, system parameters and state space equation of racing car are defined in Appendix B (See Appendix B on page 74). These three components couple m_s. to m_t. (unsprang mass of the tire). The tire is assumed to be touching the road surface permanently during the movement of the car and its stiffness is represented by the equivalent spring k_y. The vertical displacement of the head and thorax, pelvis and cushion, sprung mass, and unsprung mass are represented by z_t, z_p, z_s, and z_u, respectively. While z_r denotes the road excitation.

In matrix form, equations 9 to 12 can written as

$$\begin{bmatrix} m_t & 0 & 0 & 0 \\ 0 & m_p & 0 & 0 \\ 0 & 0 & B+m_s & -B \\ 0 & 0 & -B & B+m_u \end{bmatrix} \begin{bmatrix} \ddot{z}_t \\ \ddot{z}_p \\ \ddot{z}_s \\ \ddot{z}_u \end{bmatrix} = \begin{bmatrix} -C_t & C_t & 0 & 0 \\ C_t & -C_t-C_c & C_c & 0 \\ 0 & C_c & -C_c-C_s & C_s \\ 0 & 0 & C_s & -C_s \end{bmatrix} \begin{bmatrix} \dot{z}_t \\ \dot{z}_p \\ \dot{z}_s \\ \dot{z}_u \end{bmatrix} + \begin{bmatrix} -k_t & k_t & 0 & 0 \\ k_t & -k_t-k_c & k_c & 0 \\ 0 & k_c & -k_c-k_s & k_s \\ 0 & 0 & k_s & -k_s-k_y \end{bmatrix} \begin{bmatrix} z_t \\ z_p \\ z_s \\ z_u \end{bmatrix} + \begin{bmatrix} 0 \\ 0 \\ 0 \\ -k_y \end{bmatrix} z_y(t) \tag{13}$$

Equation (13), can be written in the following compact matrix form

$$\boldsymbol{M}\ddot{\boldsymbol{Z}} = \boldsymbol{C}\dot{\boldsymbol{Z}} + \boldsymbol{K}\boldsymbol{Z} + \boldsymbol{B}z_y(t) \tag{14}$$

According to Equation (14), $\boldsymbol{M}$**, Z,** $\dot{\boldsymbol{Z}}$**,** $\ddot{\boldsymbol{Z}}$**, C, K, and B** are given by

$$\boldsymbol{M} = \begin{bmatrix} m_t & 0 & 0 & 0 \\ 0 & m_p & 0 & 0 \\ 0 & 0 & B + m_s & -B \\ 0 & 0 & -B & B + m_u \end{bmatrix} \tag{15}$$

$$\boldsymbol{Z} = \begin{bmatrix} z_t \\ z_p \\ z_s \\ z_u \end{bmatrix}, \qquad \dot{\boldsymbol{Z}} = \begin{bmatrix} \dot{z}_t \\ \dot{z}_p \\ \dot{z}_s \\ \dot{z}_u \end{bmatrix}, \qquad \text{and } \ddot{\boldsymbol{Z}} = \begin{bmatrix} \ddot{z}_t \\ \ddot{z}_p \\ \ddot{z}_s \\ \ddot{z}_u \end{bmatrix} \tag{16}$$

$$\boldsymbol{C} = \begin{bmatrix} -C_t & C_t & 0 & 0 \\ C_t & -C_t - C_c & C_c & 0 \\ 0 & C_c & -C_c - C_s & C_s \\ 0 & 0 & C_s & -C_s \end{bmatrix} \tag{17}$$

$$\boldsymbol{K} = \begin{bmatrix} -k_t & k_t & 0 & 0 \\ k_t & -k_t - k_c & k_c & 0 \\ 0 & k_c & -k_c - k_s & k_s \\ 0 & 0 & k_s & -k_s - k_y \end{bmatrix} \tag{18}$$

$$\boldsymbol{B} = \begin{bmatrix} 0 \\ 0 \\ 0 \\ -k_y \end{bmatrix} \tag{19}$$

Solving for $\ddot{\boldsymbol{Z}}$ from Equation (14), we get

$$\ddot{\boldsymbol{Z}} = -\boldsymbol{M}^{-1}\left(\boldsymbol{C}\dot{\boldsymbol{Z}} + \boldsymbol{K}\boldsymbol{Z} + \boldsymbol{B}z_y\right) \tag{20}$$

Using the following state variable definitions,

$$\mathrm{x}_1 = \mathrm{z}_\mathrm{t}, \mathrm{x}_2 = \mathrm{z}_\mathrm{p}, \mathrm{x}_3 = \mathrm{z}_\mathrm{s}\ \mathrm{x}_4 = \mathrm{z}_\mathrm{u}$$

(21)

$$\mathrm{x}_5 = \dot{\mathrm{z}}_\mathrm{t}, \mathrm{x}_6 = \dot{\mathrm{z}}_\mathrm{p}, \mathrm{x}_7 = \dot{\mathrm{z}}_\mathrm{s},\ \mathrm{x}_8 = \dot{\mathrm{z}}_\mathrm{u}$$

The state space model of the system reads

$$\dot{\boldsymbol{x}}(t) = \boldsymbol{A}\boldsymbol{x}(t) + \boldsymbol{B_y} z_y(t) \tag{22}$$

The state vector is defined as

$$\boldsymbol{x}(\boldsymbol{t}) = \left[z_t, z_p, z_s, z_u \dot{z}_t, \dot{z}_p, \dot{z}_s, \dot{z}_u\right]^T \tag{23}$$

The system matrices $\boldsymbol{A}$, $\boldsymbol{B_y}$ are given by

(24)

$$\boldsymbol{A} = \begin{bmatrix} \mathbf{0}_{4\times4} & \boldsymbol{I}_{4\times4} \\ -\boldsymbol{M}^{-1}\boldsymbol{K} & -\boldsymbol{M}^{-1}\boldsymbol{C} \end{bmatrix},$$

(25)

$$\boldsymbol{B_y} = \begin{bmatrix} \mathbf{0}_{4\times4} \\ -\boldsymbol{M}^{-1}\boldsymbol{B} \end{bmatrix}.$$

Here, **I** and **0** denote the identity and zero matrices, respectively. Having the mathematical model, the robust multi-objective optimization problem can be formulated, and numerical simulations can be conducted to evaluate the design objectives.

2.3 Robust multi-objective optimization optimal design of the passive suspension system

We consider the RMOD of the passive suspension system of the quarter car model given by Equation (22). Four pieces of information are needed for any RMOD: the design vector, uncertainty in the decision variables, objective space, and constraints. The design vector reads

$$\boldsymbol{K} = \left[k_s, c_s, k_{y,} B\right] \tag{26}$$

Springs are responsible for supporting the vehicle and absorbing large bumps. While shock absorbers dampen the motion of the springs after a bump by dissipating energy mostly through heat. Unlike shock absorbers, inerters absorb excess energy from tires and suspension and thus reduce the effect of the oscillations and help the car to retain a better grip on the road. The calculations for uncertainty ranges are provided in Appendix C (See Appendix C on page 76). So, these are very important design parameters. The corresponding vector of uncertainties is given by

$$\boldsymbol{\delta} = \left[\delta_{ks}, \delta_{cs}, \delta_{ky,} \delta_B\right] = [5\%, 10\%, 10\%, 5\%] \tag{27}$$

The tire stiffness k_y and the shock absorber c_s experience large variations due to wear maintenance (Iroz, 2015) and (E. Abdellahi, 2001)**.** The inerter B relays on the accurate knowledge of the gear ratios, radii, and inertias, and inertia of the flywheel. Also, inerter's performance may deviate from its ideal one (Papageorgiou, 2009). As a result, we assume that the uncertainties δ_{ky} and δ_{cs} are twice that of δ_{ks} and δ_B. The objective space is defined as

$$\min_{k\in Q}\{D_s^{eff}, D_T^{eff}, a_H^{eff}\}, \tag{28}$$

where the superscript eff indicates the mean-effective value of the cost function, and a_H are the suspension deflection, tire deflection, passenger's head acceleration, respectively. According to the mathematical model given in equations 9-12, they are defined mathematically as follows:

$$D_s = z_s - z_u \tag{29}$$

$$D_T = z_u - z_r \tag{30}$$

$$a_H = \ddot{z}_t \tag{31}$$

According to Equation (29), the suspension travel describes the relative travel between the sprung mass and unsprung mass and its Root-Mean-Square (RMS) reads (Deb, 2001).

$$D_S^{RMS} = \left[\frac{1}{T}\int_0^T (D_s)^2 dt\right]^{\frac{1}{2}} \tag{32}$$

Where, T is the duration of measurement. Using the definition in Equation (7), the mean effective value of D_S is given by

$$D_s^{eff} = [\frac{1}{|\boldsymbol{B_\delta}(\mathbf{k})|} \int_{y \epsilon \boldsymbol{B_\delta}(\mathbf{k})} (D_T)^{RMS}(y)^{dy} \tag{33}$$

The Road handling is denoted by D_T which is defined as the relative travel between the unsprung mass and the road (see Equation (31). The RMS of $D_{T \text{ reads}}$

$$D_T^{RMS} = \left[\frac{1}{T}\int_0^T (D_T)^2 dt\right]^{\frac{1}{2}} \tag{34}$$

and its mean effective value is

$$D_T^{RMS} = [\frac{1}{|\boldsymbol{B_\delta}(\mathbf{k})|} \int_{y \epsilon \boldsymbol{B_\delta}(\mathbf{k})} (D_T)^{RMS}(y)^{dy} \tag{35}$$

In accordance with ISO 2631-1 (Mechanical vibration and shock; evaluation of human exposure to whole body vibration in the working environment; part 1 general requirement)**,** the RMS of the head acceleration a_H is given by

$$a_H^{RMS} = \left[\frac{1}{T}\int_0^T (a_H)^2 dt\right]^{\frac{1}{2}} \tag{36}$$

Similarly, its mean effective value is given by

$$a_H^{eff} = \frac{1}{(\,|\boldsymbol{B_\delta}(\boldsymbol{k})|\,)} \int_{y \in \boldsymbol{B_\delta}(\boldsymbol{k})} a_H^{RMS}\,(y) dy \tag{37}$$

The decision variables' search space is constrained to the following region:

$$Q = \{\, k \ \in [150 \ \times 10^3, 450 \ \times 10^3] \ \times [4 \ \times \ 10^{3,12} \times 10^3] \times [116.5 \ \times \ 10^{3,345} \times 10^3] \times [\ 116.5 \ \times \ 10^{3,345} \times 10^3] \times [0,4] \subset \mathbb{R}^4\} \tag{38}$$

The ranges of k_S and k_Y are chosen as $k_{SN} \ \times \ [0.5,1.5] \ and \ k_{YN} \times \ [0.5,1.5]$, respectively, where $k_{SN} \ = 300$ kN /m and $k_{YN} \ = 233\text{kN/m}$ (Bulman, 1997). The ranges of c_s, and B are specified from the engineering point of view of suspension deflection (Kuznetsov, Mammadov, Sultan, & Hajilarov, 2011). Furthermore, constraints are imposed on the objective space. According to (A. Baumal, 1998) and (Nagarkar, Patil, & Patil, 2016)**,** the maximum suspension travel should be 125 mm to avoid hitting the suspension stop and the maximum a_H should be less than or equal to 4.5 m/s^2. For better tire gripping, the maximum deflection should not increase 58 mm.

In the numerical simulation, z_y is modeled as a bump of height 0.1 unit (Nagarkar et al., 2016). The parameters are set as $m_t = 2\text{m}/7$ kg, $m_p = 5\text{m}/7$ kg, ct $= 1360$ N. s/m, kt $=$ 45005.3 N/m, cc $= 900$ N. s/m, $k_c = 10000$ N/m, and $m_u = \ 20$ kg, where m $=$ 65 kg (Kuznetsov et al., 2011). The sprung mass m_s is set to 180 kg (Bulman, 1997)**.** This value is very close to the quarter mass of the 2017 Formula 1(F1) car, which was about 728kg according to motorsport. However, in 2018, the mass was increased to 734 kg after adding the Halo (driver crash protection system). In order to follow the design method introduced in this thesis, designers should adjust m_s based on the weight of the car on which they are working. To solve this multi-optimization problem, NSGA-II is used. Due to space limitations, the reader can refer to (Deb, 2001) for more details about this algorithm. It was shown by Deb and Gupta (Deb & Gupta, Introducing robustness in multi-objective optimization, 2006) that the algorithm is efficient in finding robust solutions of benchmark problems with two and three objectives.

There is not a clear guide about setting up the number of populations and generations for NSGA-II. However, according to the MATLAB documentation, the population size can be set in different ways and the default population size is 15 times the number of the design variables. Also, the maximum number of generations should not exceed 200× design variables. In this study, the population size and the number of generations is set to $50 \times$ design variables. For comparison purposes, the global Pareto solutions were also obtained using the same settings. In terms of the robust solution, a finite set of 20 solutions are randomly created within the neighborhood of the design parameters to account for their expected variations and calculate the mean effective objectives.

2.5 Results and Discussion

The global and robust Pareto fronts and sets and robustness of the suspension system in terms of the objective functions are discussed here. The optimization process results in 200 various solutions which means there are 200 different optimal and robust suspension configurations with different trade-offs among the design objectives. Projections of the global and mean-effective fronts are shown in Figures 3 and 4. The corresponding Pareto sets are shown in 5 and 6. The yellow color in these figures denotes the feasible regions in the objective and parameter space defined in Equation (38). The global and robust solutions are represented by the black star and blue dot, respectively. Both global and robust Pareto fronts demonstrate competing relationships among the design goals, which emphasizes the necessity of carrying out the design of the passive suspension system in multi-objective settings. The results also show that both global and robust regions are inside the feasible zone and the robust Pareto frontier avoids all the boundaries. Taking the robust Pareto front as an example, we notice that when $D_S^{eff} = 0.0039$ (maximum value), D_T^{eff} and a_H^{eff} read 0.0036 and 3.1182 respectively. While at the minimum value of D_S^{eff}=0.0021, D_T^{eff}=0.0072 and a_H^{eff}=3.6023. Meaning, both D_T^{eff} and a_H^{eff} objectives increases when D_S^{eff} goes down and vice versa as it is evident from Figures 13 and 14. Between these two design options, there are many robust and optimal options that the decision-maker can choose to implement. It should be indicated that the smaller a_H^{eff}, the better. Small values of a_H^{eff} mean that the amount of the transmitted forces to the pelvis and thorax is the lowest. The optimization algorithm offers 200 global and robust solutions. Therefore, it is not practical to compare the robustness of the global Pareto front and mean effective Pareto frontier for all the solutions. Instead, two solutions from the robust and global Pareto set are chosen randomly. Then, a random perturbation is generated according to the uncertainty vector defined in equation (27). After that, the same amount of perturbation is added to both solutions. Finally, the profiles of the absolute error between the perturbed and nonperturbed solutions for both global and robust solutions are depicted in Figures (16)-(21). The deviations in the suspension traveling terms of its global ((E_{Ds}) |G) and robust (|E_{Ds} |R) values are defined as follows

$$|E_{Ds}|_{\mathrm{G}} = |D_{sG} - D_{sGP}|, \tag{39}$$

$$|E_{Ds}|_{\mathrm{R}} = |D_{sR} - D_{sRP}|. \tag{40}$$

Where, D_{sG} and D_{sR} Represent the global and robust $\mathrm{D_s}$ with no variations in the design parameter and D_{sGP} and D_{sRP} denote their corresponding values as result of parametric uncertainties. Similarly, the deviations in the global and robust responses of $\mathrm{D_T}$ and a_H can be defined in the following equation

$$|E_{\mathrm{D_T}}|_{\mathrm{G}} = |D_{TG} - D_{TGP}| \tag{41}$$

$$|E_{\mathrm{D_T}}|_{\mathrm{R}} = |D_{TR} - D_{TRP}| \tag{42}$$

$$|E_{a_H}|_{\mathrm{G}} = |a_{HG} - a_{HGP}| \tag{43}$$

$$|E_{a_H}|_{\mathrm{R}} = |a_{HR} - a_{HRP}| \tag{44}$$

Where, the subscripts G, R, and P mean respectively global, robust, and perturbed. As evident from these Figures (16) - (21), the global profiles of D_S, D_T, and a_H are more sensitive to the perturbation than the robust ones. This stresses out the need to handle the problem at hand in robust settings.

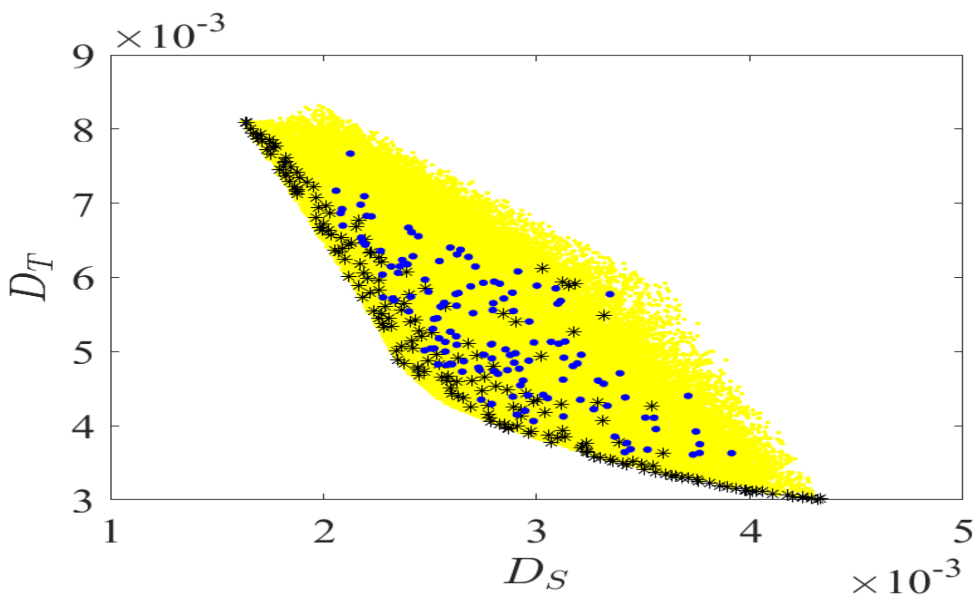

Figure 4. *Projection # 1 of the global and robust Pareto front (D_T versus D_S). Yellow region: feasible Pareto front, black (*): global Pareto front, and blue (·): robust Pareto front.*

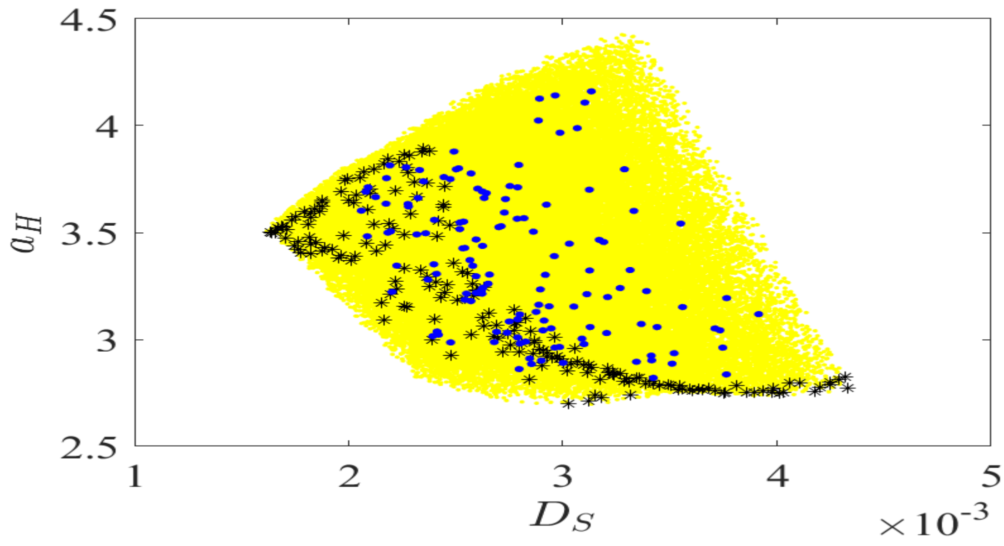

***Figure* 5.** *Projection # 2 of the global and robust Pareto front (a_H versus D_S). Yellow region: feasible Pareto front, black (*): global Pareto front, and blue (·) : robust Pareto front.*

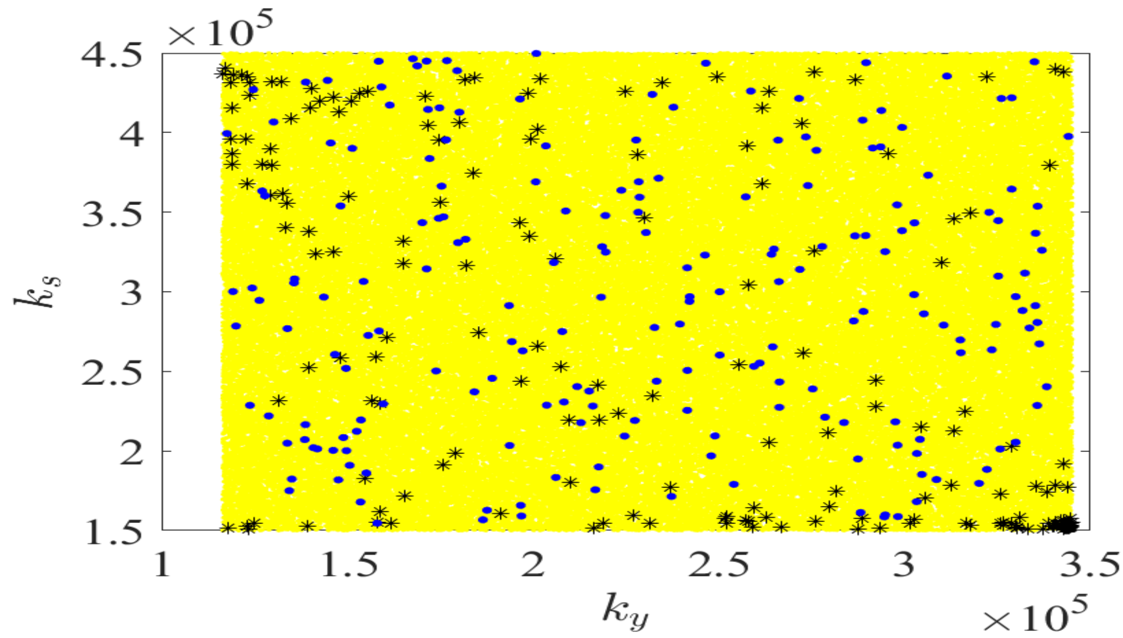

***Figure* 6.** *projection # 1 of the global and robust Pareto set (($k_s$versus k_y).Yellow region: feasible Pareto set, black (*): global Pareto set, and blue·: robust Pareto set.*

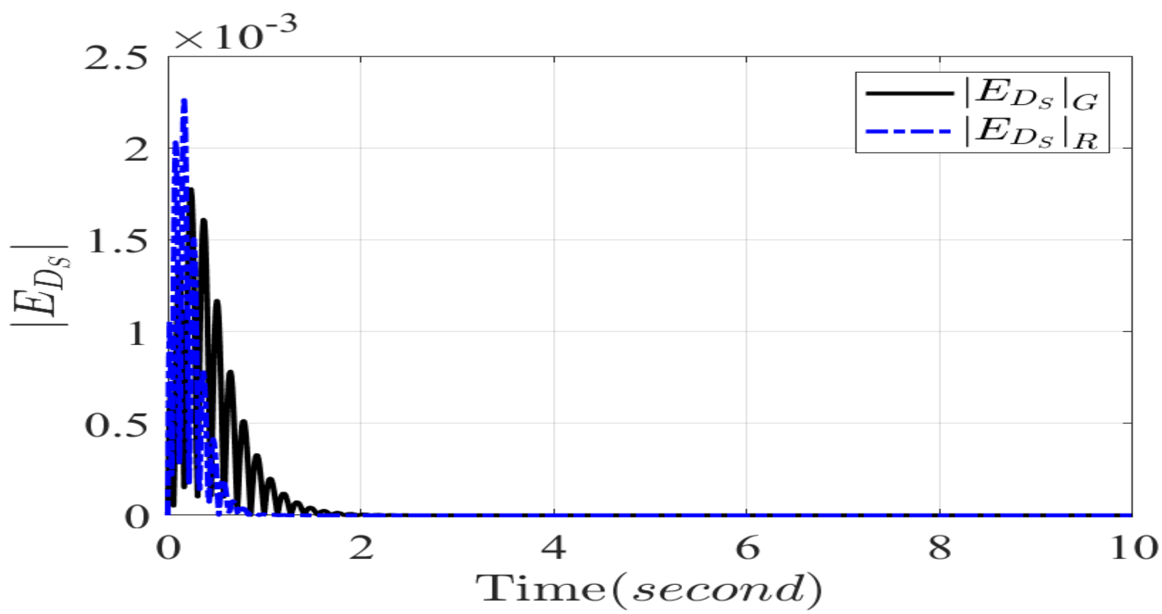

***Figure* 7.** *: profiles of the absolute deviations in the suspension travel $|E_{Ds}|$ for the perturbed non perturbed global ($|E_{Ds}|_G$) and robust ($|E_{Ds}|_R$)solutions from the first randomly selected solution.*

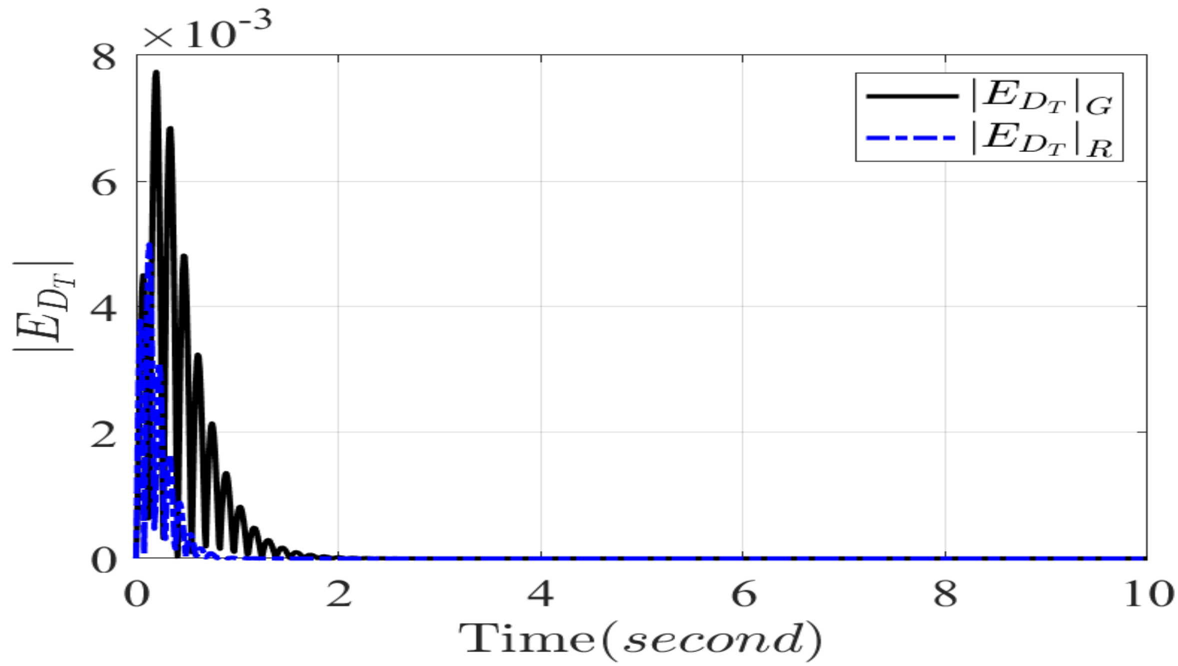

***Figure* 8.** *profiles of the absolute deviations in the suspension travel* $|E_{Ds}|$ *for the perturbed and non-perturbed global* ($|E_{Ds}|_G$) *and robust* ($|E_{Ds}|_R$) *solutions from the second randomly selected solution*

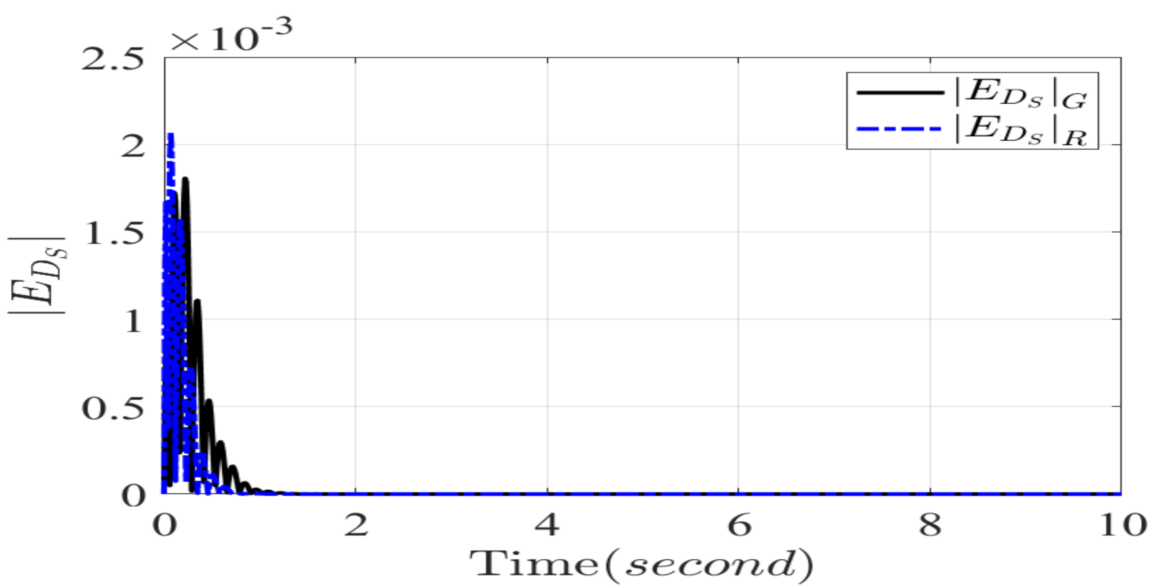

***Figure* 9.** *Profiles of the absolute deviations in the tire travel* $|E_{DT}|$ *for the perturbed and non-perturbed global* ($|E_{DT}|_G$) *and robust* ($|E_{DT}|_R$) *solutions from the first randomly selected solution.*

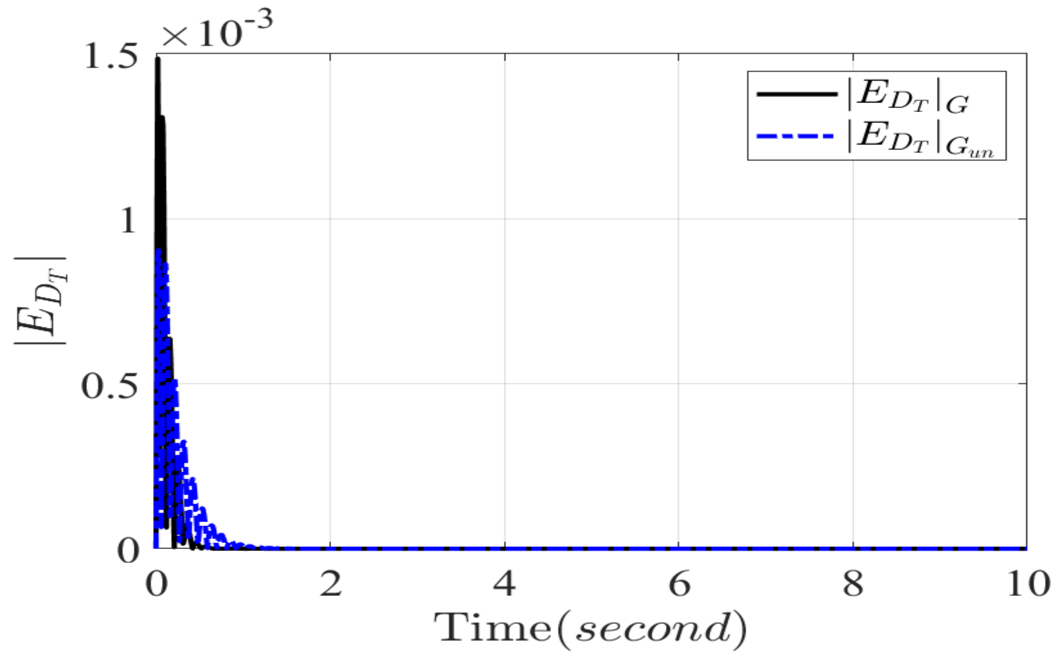

***Figure* 10.** *Profiles of the absolute deviations in the tire travel* $|E_{DT}|$ *for the perturbed and non-perturbed global* ($|E_{DT}|_G$) *and robust* ($|E_{DT}|_R$) *solutions from the second randomly selected solution.*

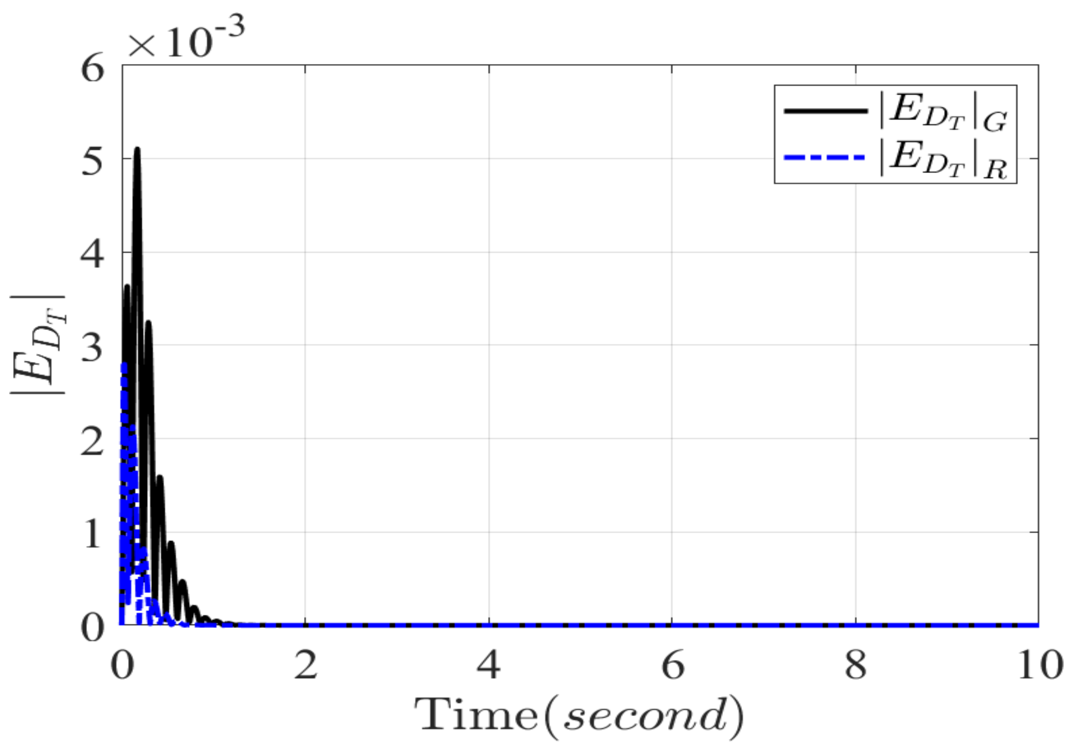

***Figure* 11.** *Profiles of the absolute deviations in the head acceleration* $|Ea_H|$ *for the perturbed and non-perturbed global* ($|Ea_H|_G$) *and robust* ($|Ea_H|_R$) *solutions from the first randomly selected solution.*

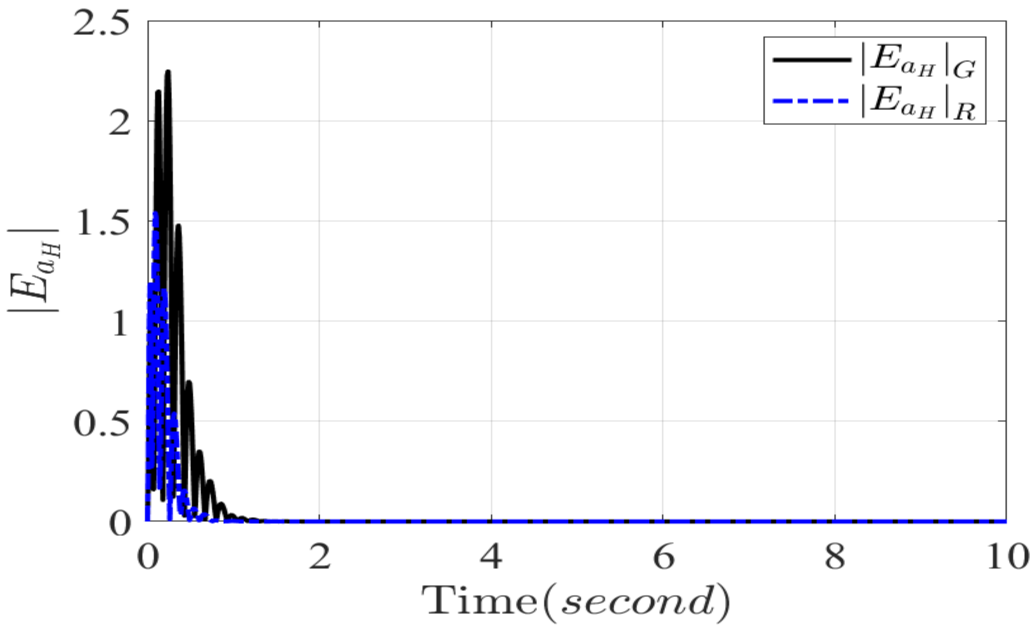

Figure 12. *Profiles of the absolute deviations in the head acceleration $|Ea_H|$ for the perturbed and non-perturbed global ($|Ea_H|_G$) and robust ($|Ea_H|_R$) solutions from the first randomly selected solution.*

2.6 Conclusion

We have studied the RMOD of a passive suspension system with an inerter device. The optimization problem with 4 design parameters and 3 objective functions is solved by the NSGA-II algorithm. The global and robust Pareto set, and front are obtained. The Pareto set includes multiple design options from which the decision-maker can choose to implement. Numerical simulations show that the robust multi-objective design (RMOD) is very effective and guarantees a robust behavior as compared to that of the classical multi-objective design (MOD). The results also show that the robust region is inside the feasible objective space and avoids all its boundaries. Also, the results show that the design goals are competing, and as a result, there are many optimal and robust passive suspensions with different degrees of compromises among the design objectives. As expected, the numerical simulations manifest that the solutions from the robust Pareto set are more robust than those from the global set.

CHAPTER 3: MULTI-OBJECTIVE ROBUST DESIGN OF A PASSENGER SPORTS CAR WITH SEMI-ACTIVE SUSPENSION SYSTEM

3.1 Introduction

This chapter presents a robust multi-objective optimal design (RMOP) of a passenger car with a semi-active suspension system. The mean-effective values of the root mean square of passenger's head acceleration, suspension travel, and tire deflection are considered as design objectives. The passive components of the suspension and the design details of the Linear Quadratic Regulator (LQR) algorithm are used as design parameters. During the design, global sensitivity analysis is carried out using the Fourier Amplitude Sensitivity Test (FAST) to specify the elements of the model that can highly alter the design objectives. The mass of the passenger's head and upper body, the mass of the passenger's lower body and cushion, passenger and cushion's elastic properties, and the sprung mass of the vehicle are selected for the sensitivity analysis. Results show that the design criteria are very sensitive to the variations in the sprung mass of the vehicle compared to the other parameters. As a result, the variations in this parameter and passive elements of the suspension system are considered. Similar to the design of passive suspension system, constraints are applied on the objectives in compliance with the requirements of ISO 2631-1 on the design of car suspension systems. The optimization problem is solved by the NSGA-II and robust Pareto front and set are obtained. The car mathematical model, control system design, formulation of the multi-objective problem, sensitivity analysis, and the results of the optimization problem are introduced in the next sections.

3.2 Commercial Car Model

A quarter car model of a passenger car implementing a semi-active suspension system is shown in Figure (13). In this model, the passenger is modelled as a two-degree-of-freedom system by splitting the passenger's body mass into two parts: m_t and m_p such that m_p is connected to m_t by an assumed spring k_t and damper c_t. The cushion's elastic properties are modeled as an equivalent spring k_c and damper c_c which couple m_p to the sprung mass m_s. The suspension system is modeled as a spring with constant k_s, and damper with coefficient c_s. These system parameters and matrices are defined in Appendix D (See Appendix D on page 78). The control force, $u(t)$, is calculated by the LQR algorithm assuming that the vertical displacement of the sprung and un-sprung masses (z_s and z_u) and their derivatives (dz_s/dt and dz_u/dt) are available for feedback. The modeling equations of the system read

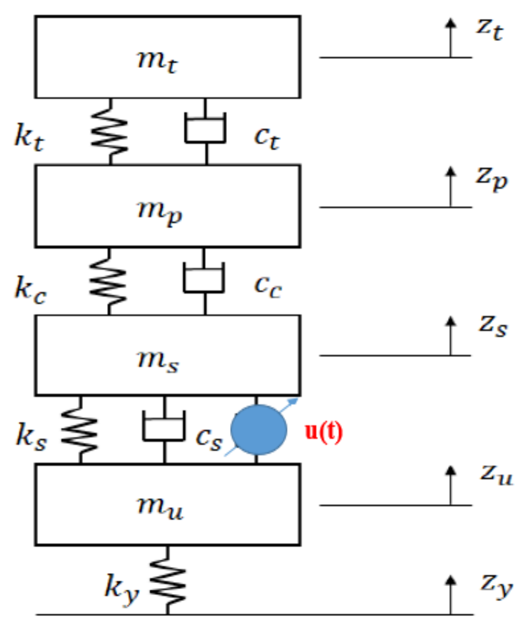

Figure 13. *Commercial car model with semi active suspension system.*

$$m_t\ddot{z}_t = -c_t\left(\dot{z}_t - \dot{z}_p\right) - k_t\left(z_t - z_p\right),$$

$$m_p\ddot{z}_p = c_t\left(\dot{z}_t - \dot{z}_p\right) + k_t(z_t - z_p) - c_c(\dot{z}_p\text{-}\dot{z}_s) - k_c(z_p - z_s),$$

$$m_s\ddot{z}_s = c_c(\dot{z}_p\text{-}\dot{z}_s) + k_c(z_p - z_s) - c_s(\dot{z}_s - \dot{z}_u) - k_s(z_s - z_u) + u(t) \tag{45}$$

$$m_u\ddot{z}_u = c_s(\dot{z}_s - \dot{z}_u) + k_s(z_s - z_u) - k_y(z_u - z_y) - u(t)$$

If the seat and the driver are not included, the model reads

$$m_s\ddot{z}_s = -c_s(\dot{z}_s - \dot{z}_u) - k_s(z_s - z_u) + u(t) \tag{46}$$

$$m_u\ddot{z}_u = c_s(\dot{z}_s - \dot{z}_u) + k_s(z_s - z_u) - k_y(z_u - z_y) - u(t)\ ,$$

which can be written as

$$\ddot{z}_s = -\frac{k_s}{m_s}z_s + \frac{k_s}{m_s}z_u - \frac{c_s}{m_s}\dot{z}_s + \frac{c_s}{m_s}\dot{z}_u + \frac{1}{m_s}u(t)$$

$$\ddot{z}_u = \frac{k_s}{m_u}z_s - \left(\frac{k_s}{m_u} + \frac{k_y}{m_u}\right)z_u + \frac{c_s}{m_u}\dot{z}_s - \frac{c_s}{m_u}\dot{z}_u + \frac{k_y}{m_u}z_y - \frac{1}{m_u}u(t) \tag{47}$$

Defining the state-vector $\boldsymbol{x_s} = [x_1 \quad x_2 \quad x_3 \quad x_4]^T = [z_s \quad z_u \quad \dot{z}_s \quad \dot{z}_u]^T$,

the state variable equations are given by,

$$\dot{x}_1 = x_3$$

$$\dot{x}_2 = x_4$$

$$\dot{x}_3 = -\frac{k_s}{m_s}x_1 + \frac{k_s}{m_s}x_2 - \frac{c_s}{m_s}x_3 + \frac{c_s}{m_s}x_4 + \frac{1}{m_s}u(t) \tag{48}$$

$$\dot{x}_3 = \frac{k_s}{m_u}x_1 - \left(\frac{k_s}{m_u} + \frac{k_y}{m_u}\right)x_2 + \frac{c_s}{m_u}x_3 - \frac{c_s}{m_u}x_4 + \frac{k_y}{m_u}z_y - \frac{1}{m_u}u(t)$$

The matrix representation of these equations is given by,

$$\begin{bmatrix}\dot{x}_1\\ \dot{x}_2\\ \dot{x}_3\\ \dot{x}_4\end{bmatrix} = \begin{bmatrix} 0 & 0 & 1 & 0\\ 0 & 0 & 0 & 1\\ -\frac{k_s}{m_s} & \frac{k_s}{m_s} & -\frac{c_s}{m_s} & \frac{c_s}{m_s}\\ \frac{k_s}{m_u} & -\left(\frac{k_s}{m_u}+\frac{k_y}{m_u}\right) & \frac{c_s}{m_u} & -\frac{c_s}{m_u}\end{bmatrix}\begin{bmatrix}x_1\\ x_2\\ x_3\\ x_4\end{bmatrix} + \begin{bmatrix}0\\ 0\\ 0\\ \frac{k_y}{m_u}\end{bmatrix} z_y(t) + \begin{bmatrix}0\\ 0\\ \frac{1}{m_s}\\ \frac{-1}{m_u}\end{bmatrix} u(t) \tag{49}$$

A compact state-space model read

$$\dot{\boldsymbol{x}}_{\boldsymbol{s}}(t) = \boldsymbol{A}\boldsymbol{x}_{\boldsymbol{s}}(t) + \boldsymbol{B}_{\boldsymbol{y}} z_y(t) + \boldsymbol{B}_{\boldsymbol{u}} u(t) \tag{50}$$

This model will be used in the next section in the design of the control system.

3.3 Control Design

The control force $u(t)$ can be designed in different ways. One of the popular methods in classical optimal control is the Linear Quadratic Regulator (LQR). The control force is given by,

$$u(t) = -\mathbf{K_s}\mathbf{x_s}(t), \tag{51}$$

The optimal state feedback control gain matrix $\mathbf{K_s}$ can be obtained by minimizing the following quadratic cost function:

$$\mathrm{J} = \int_0^\infty [\mathbf{x}^T(t)\mathbf{Q}\mathbf{x}(t) + \mathrm{u}^T(t)\mathbf{R}\mathrm{u}(t)]\, dt, \tag{52}$$

where $\mathbf{Q} = \mathbf{Q}^{\mathrm{T}}$ is a positive semidefinite matrix that penalizes the departure of system states from their equilibria, and $\mathbf{R} = \mathbf{R}^{\mathbf{T}}$ is a positive definite matrix that penalizes the control force. Using Lagrange multiplier-based optimization method, the optimal $\mathbf{K_s}$ is given by

$$\boldsymbol{K_s} = \mathbf{R}^{-1}\boldsymbol{BP} \tag{53}$$

The matrix $\boldsymbol{P} \in \Re^{4\times4}$ can be calculated by solving the following Algebraic Riccati Equation (ARE):

$$\mathbf{A^T P + PA - Q - PBR^{-1}B^T P = 0} \tag{54}$$

Inspecting Eqs. (53) and (54), we can notice that the choice of **Q** and **R** will greatly affect the performance of the controlled system. Thus, these weighting matrices need to be tuned. Traditionally, **Q** and **R** are chosen based on the expert of the control system designer and tweaked iteratively to achieve the design requirements. Arbitrary settings of **Q** and **R** may result in non-optimal performance. The state space model and control design are defined in Appendix E (See Appendix E on page 80). Many works have been proposed about establishing systematic approaches for calculating **Q** and **R**. For example, Bryson developed a method for selecting these matrices, but his method shows only how the initial values should be selected and the designer still needs to tune the elements of **Q** and **R** for optimal performance (Bryson, 2018). Other examples can be found in (Oral, Çetin, & and Uyar, 2010) and (El Hajjaji & Ouladsine, 2001). Therein, analytical methods for selecting **Q** and **R** for second order and third-order systems were developed. So, these techniques cannot be used to calculate **Q** and **R** for the control algorithm applied to the semi-active suspension system because of its dimensionality. Hence, we suggest a numerical approach to tackle this problem.

3.4 Robust multi-objective optimization optimal design of the semi-active suspension system

We consider the RMOD for the semi-active suspension system. The design vector reads

$$\boldsymbol{K} = [k_s, c_s, k_{y,} Q_1, \dots, Q_4, R]. \tag{55}$$

The variables $k_s, c_s,$ and k_y are the passive elements of the suspension system shown in Figure (13). The variables $Q_1, \dots, Q_4$, are the diagonal elements of **Q**, and R is the control force weighting factor. The constraints on the design parameter space are given by

$$
\boldsymbol{D} = \left\{ \begin{array}{c} \boldsymbol{k} \in \mathfrak{R}^8 |\ Q_1, Q_2, Q_3, Q_4 \in [0,100], \\ R \in [1.0 \times 10^{-6}, 100], \\ k_y \in [95,285] \times 10^3 , \\ k_s \in [11750,35250], \\ c_s \in [350,1050] \end{array} \right\} \tag{56}
$$

The upper bounds of $Q_1 Q_2, Q_3, Q_4,$ and R are chosen so that the penalties on the departures of the states from their desired positions and control utilization are high. The upper and lower bounds of $k_y, k_s,$ and c_s were chosen according to the work presented in (Nagarkar, Patil, & Patil, 2016).

The tire stiffness depends on the inflation pressure and road temperature. It also varies from one manufacturer to another. Furthermore, k_y changes due to wear while it is in service. To account for these factors, k_y variations are initialized ($k_y \pm \delta_{ky} k_y$) (Loyer & Jézéquel, 2009), where $\delta_{ky} = 10\%$. The spring and damping coefficients of the suspension system will degrade during the service due to aging and wear and their values will decrease over time. To simulate these variations, k_s and c_s uncertainties are defined as follows

$$
\delta_{ks} \in [-25\%, 0\%] \tag{57}
$$

$$
\delta_{cs} \in [-25\%, 0\%] \tag{58}
$$

The design parameters defined in Equation (55) with their constraints given in Equation (56) and by considering $\delta_{ky}, \delta_{ks},$ and δ_{cs} are tuned to concurrently satisfy three objectives:

$$
\min_{k \in Q} \{D_s^{eff}, D_T^{eff}, a_H^{eff}\}. \tag{59}
$$

Where, D_s^{eff}, D_T^{eff}, and a_H^{eff} are respectively the mean-effective value of the suspension stroke, D_s, the tire deflection, D_T, and head acceleration a_H. Elaborated discussion of these objectives can be found in Section 3.4.

It is obvious that the environmental and operational variabilities of k_y, k_s, and c_s can be simulated by considering their uncertainties δ_{ky}, δ_{ks}, and δ_{cs}. But the question is: can the variations in the other system parameters, namely m_t, m_p, k_t, c_t, k_c, c_c, and m_s, alter the design objectives? To answer this question, sensitivity analysis is conducted.

3.5 Fourier Amplitude Sensitivity Test (FAST)

Fourier Amplitude Sensitivity Test (FAST) is based on the Fourier transformation of the uncertain model's input parameters into frequency domain. The algorithm provides with the most suitable computational efficiency to conduct global sensitivity analysis (GSA). The algorithm starts with calculating the uncertainty ranges of the input variables. Then, a unique frequency is assigned to each input parameter as shown in Figure 14. This frequency assignment is achieved by the conversion of multi-dimensional integral to one-dimension integral using Fourier series (Lehman & Stoilov, 2015). The amplitude of frequencies obtained is used to indicate the effect of each parametric variation on a certain cost function. The obtained Fourier coefficients, calculations are provided in Appendix G (See Appendix G on page 83) are applied to calculate the partial variance of individual parameters of the system. The total variance for each input is thus calculated by computing the overall variances of the system.

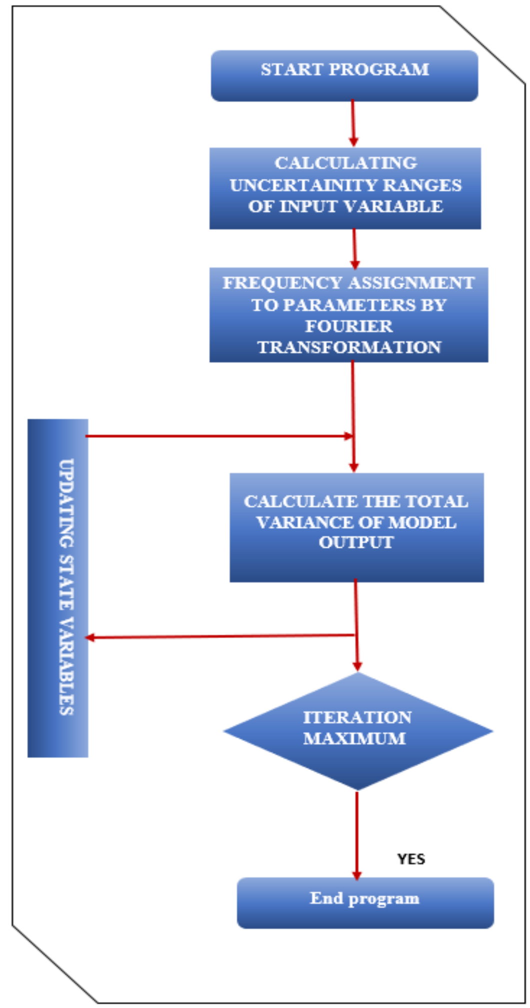

Figure 14: *Flow chart of Fourier Amplitude Sensitivity Test (FAST)*

3.5 Global Sensitivity Analysis (GSA)

Global sensitivity analysis (GSA) is performed by using the Fourier Amplitude Sensitivity Test (FAST) based on Monte Carlo sampling, which is one of the commonly used methods for sensitivity analysis. The uncertainties in m_t, $m_p, k_t,$ and c_t are set to $\pm 20\%$. The seat spring k_c and damper c_c is set between $[\ k_c - 0.1\ k_c\ ,\ k_c]$ and $[\ c_c - 0.1 c_c,\ c_c]$, respectively. The sprung mass m_s fluctuates due to the variation of car occupants and luggage. The sprung mass, m_s is set to between 10% variations ($m_s \pm 0.1 m_s$) (Qin, Wang, Yuan, & Zhang, 2019). The sensitivity indices of the seven parameters are demonstrated for the root mean square value (RMS) of the suspension deflection $\mathrm{S_D^{RMS}}$, occupant's head acceleration $\mathrm{a_H^{RMS}}$, and tire deflection $\mathrm{T_D^{RMS}}$. Furthermore, the sensitivities of these objectives are evaluated at different levels of the control force. Figures (15) and (16) show respectively the sensitivity indices when $u(t)$ is large (the settings of the LQR algorithm are: $R = 1.0 \times 10^{-6}, Q_1 = Q_2 = Q_3 = Q_4 = 100$) and when $u(t)$ is small (LQR settings: $R = 100, Q_1 = Q_2 = Q_3 = Q_4 = 0$). Similarly, Figures (17) and (18) display the sensitivity indices at these different control forces. It is evident from these figures that $\mathrm{S_D^{RMS}}$and $\mathrm{T_D^{RMS}}$ are mainly affected by the variations of $m_s, m_p,$ and m_t, but m_s is recording the highest impact. The upper bound of noise parameters are defined in Appendix F (See Appendix F on page 81). The other four parameters $\mathrm{c_t}, \mathrm{c_c}, \mathrm{k_c}$ and $\mathrm{k_t}$ have almost no affect $\mathrm{S_D^{RMS}}$and $\mathrm{T_D^{RMS}}$, and hence are neglected. In a similar fashion, the sensitivity indices of the model variables are calculated for $\mathrm{a_H^{RMS}}$ at large $u(t)$ and small $u(t)$ and are depicted in Figures (19) and (20), respectively. The figures demonstrate that $\mathrm{a_H^{RMS}}$ is insensitive to these elements.

To sum up, it is obvious that the deviations in m_s will certainly influence the values of two cost functions from the selected three design objectives. As a result, m_s is varied during the optimization to find less sensitive and robust solutions to the optimization problem at hand.

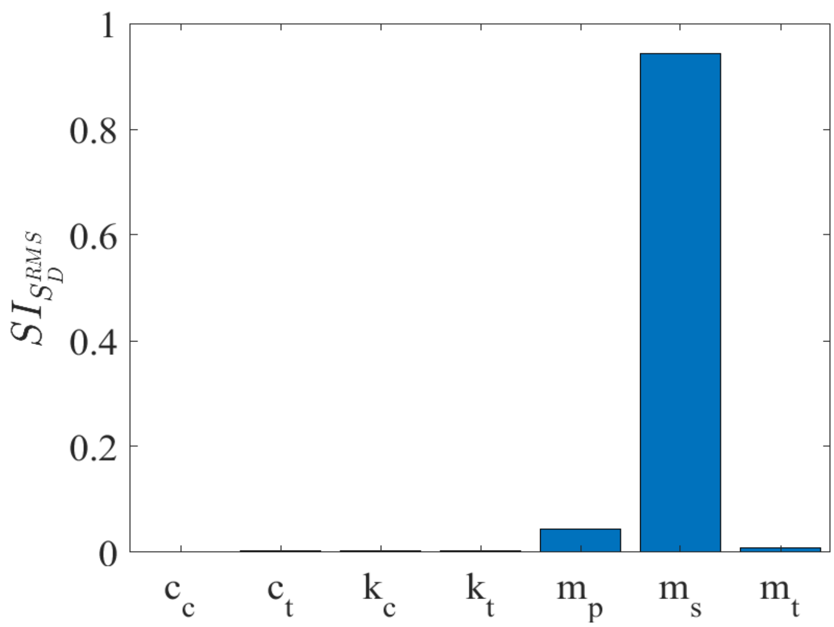

Figure 15: *Sensitivity indices of the sprung mass, and body and seat elements on S_D^{RMS} when u(t) is large.*

.

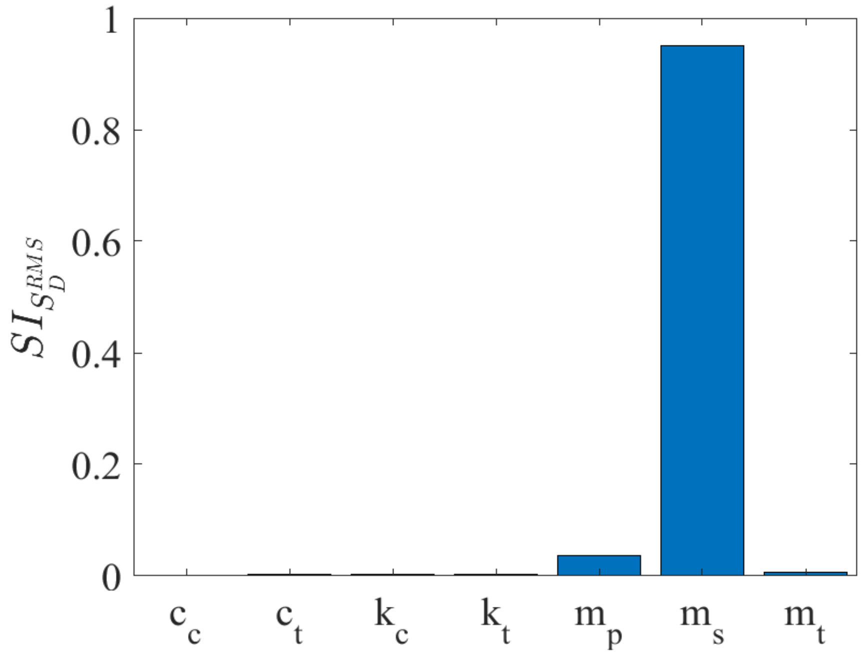

Figure 16 : *Sensitivity indices of the sprung mass, and body and seat elements on* S_D^{RMS} *when u(t) is small.*

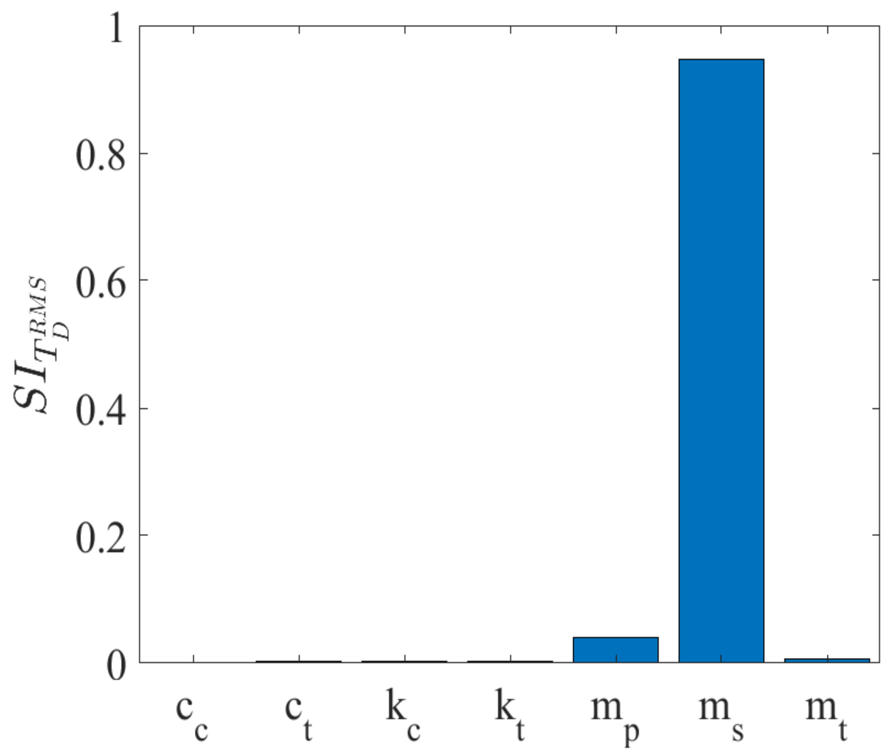

Figure 17: *Sensitivity indices of the sprung mass, and body and seat elements on T_D^{RMS} when u(t) is large.*

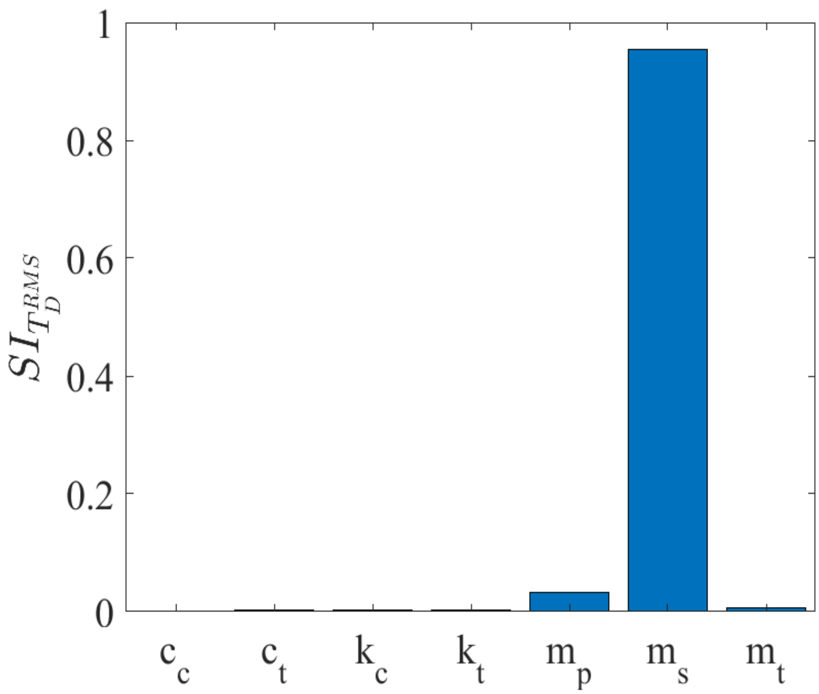

Figure 18: *Sensitivity indices of the sprung mass, and body and seat elements on T_D^{RMS} when u(t) is small.*

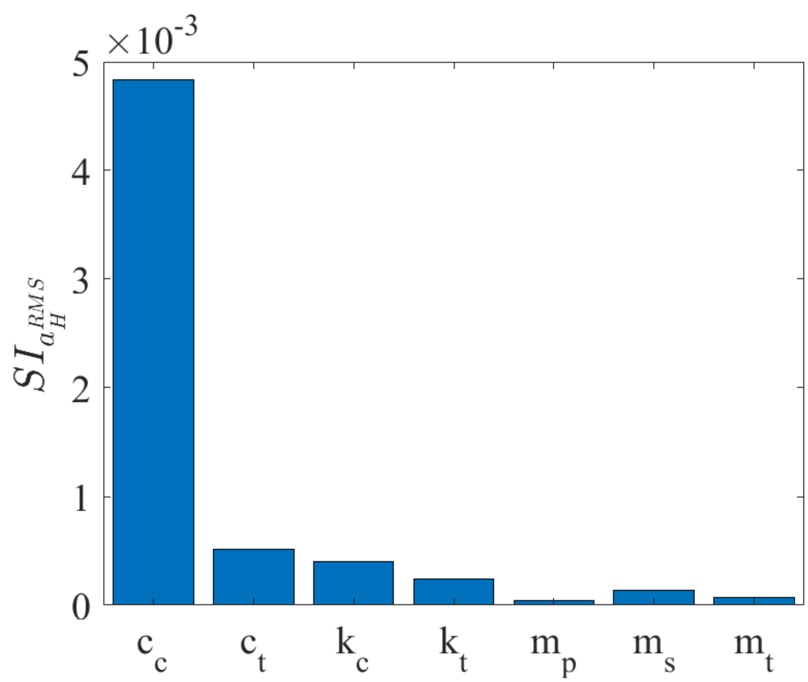

Figure 19: *Sensitivity indices of the sprung mass, and body and seat elements on a_H^{RMS} when u(t) is large.*

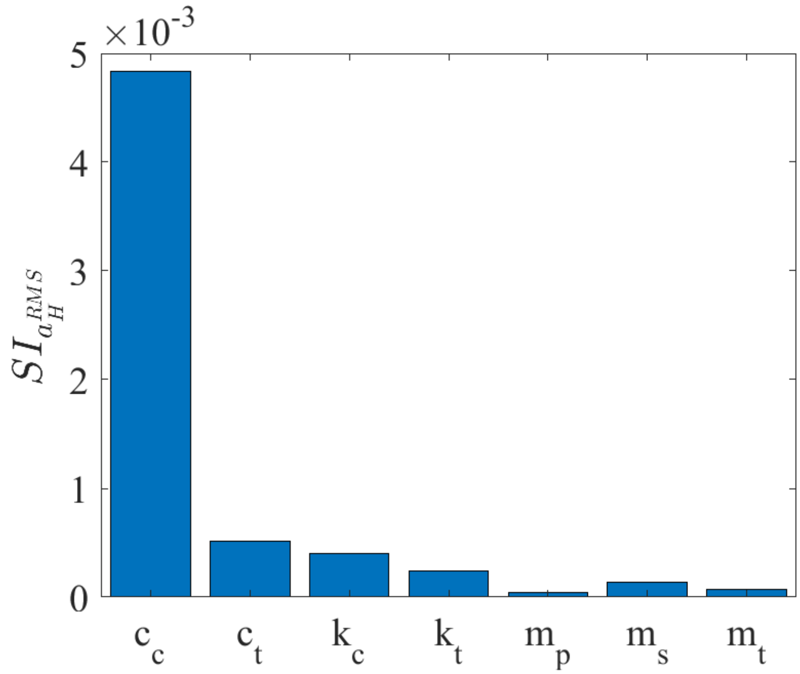

Figure 20: *Sensitivity indices of the sprung mass, and body and seat elements on a_H^{RMS} when u(t) is small.*

To solve this multi-optimization problem, the NSGA-II is used; the reader can refer to Section 1.4 for more details about this algorithm. During the optimization, the population size is set to 50 and the maximum number of function evaluations is set to 1000. For the robust solution, a finite set of 20 solutions are randomly created within the neighborhood of the nominal values of $k_y, k_s, c_s,$ and m_s. Then, the mean effective values of the objective functions are calculated. The quarter-car model is simulated with MATLAB using ode15s for 10 seconds with a step size of 10 milliseconds. During the numerical simulation, the nominal value of m_s is set to 290 kg. According to (Kuznetsov et al., 2011), other parameters can be set to: $m_p = 46.43\ kg$, $m_t = 18.57\ kg$, $k_t = 45005.3\ N/m$, $c_t = 1360\ N.s/m$, $k_c = 10000 N/m$, and $c_c = 900\ N.s/m$. The road profile z_y is chosen as a sinusoidal shape with two successive slopes of depth of $h = 0.05\ m$, and length $\lambda = 20\ m$ as shown in Figure (21) (Shirahatti, Prasad, Panzade, & Kulkarni, 2008). The vehicle velocity V is $v = 20\ m/s$. In mathematical terms, z_y is given by

$$z_y = \begin{cases} \frac{h}{2}\left(1 - \cos\left(\frac{2\pi v}{\lambda}t\right)\right), & if\ 0 \leq t \leq \frac{2\lambda}{v} \\ 0, & otherwise \end{cases} \quad (60)$$

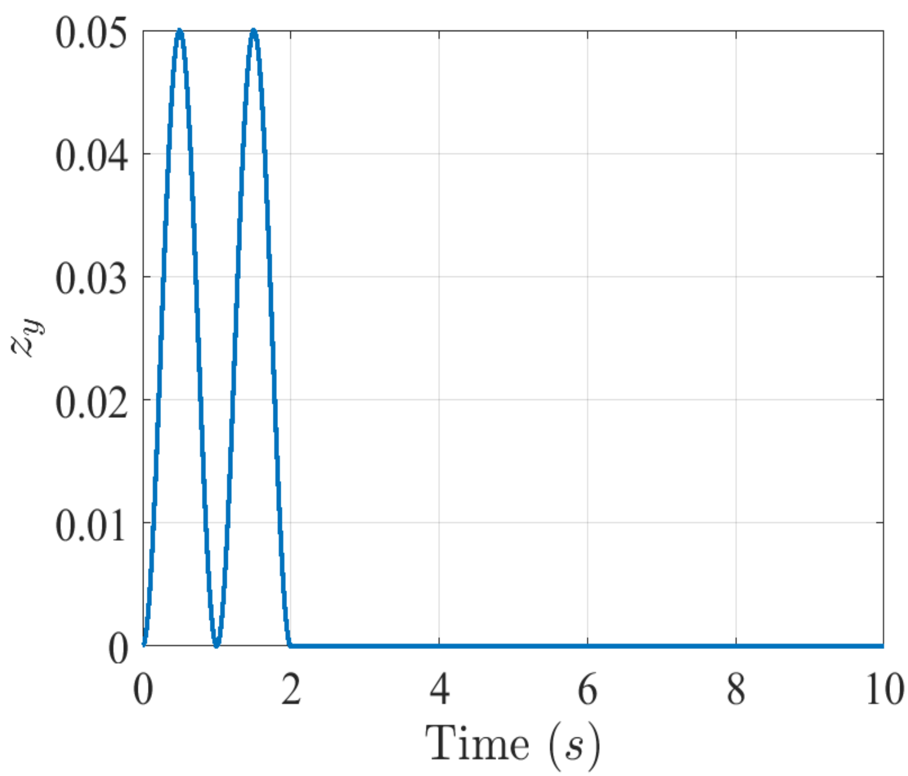

Figure 21*: Road Profile*

Under these conditions, the robust multi-objective optimization problem is solved and its solution in terms if robust Pareto front and set are obtained.

3.6 Results and Discussion

Projections of the robust Pareto front are shown in Figures (22) and (23). The robust trade-offs between the effective-mean of the head acceleration and that of the suspension deflection (a_H^{eff} versus D_s^{eff}) are depicted in Figure (22), while those between the suspension deflection and tire deflection (D_s^{eff} versus D_T^{eff}) are plotted in Figure (23). Both projections exhibit competing relationships among the design objectives. For instance, by inspecting Figure (22), we notice that a_H^{eff} decreases as D_s^{eff} goes up. Similarly, D_T^{eff} goes down as D_s^{eff} increases. The competing nature of these objectives stresses out the fact that these objectives need to be handled in multi-objective settings. Projections of the corresponding Pareto sets are graphed in Figure (24). The optimal passive components ($\mathrm{c_s}$ versus $\mathrm{k_s}$ and the color is mapped to the value of $\mathrm{k_y}$) are depicted in Figure (24-a). The subplot shows that higher values of $\mathrm{c_s}$ are associated with higher levels of $\mathrm{k_y}$. While the active design parameters of the suspension systems are plotted in subfigures (b) and (c). The color in these subfigures is mapped to the level of the control penalizing factor, R. These subplots demonstrate that the weighting elements of the LQR algorithm within the feasible ranges and different optimal solutions that can be found by optimal adjustment. In order to show the robustness of these solutions, time-domain profiles of the suspension deflection, tire deflection, and head acceleration at random point from the Pareto set are discussed next.

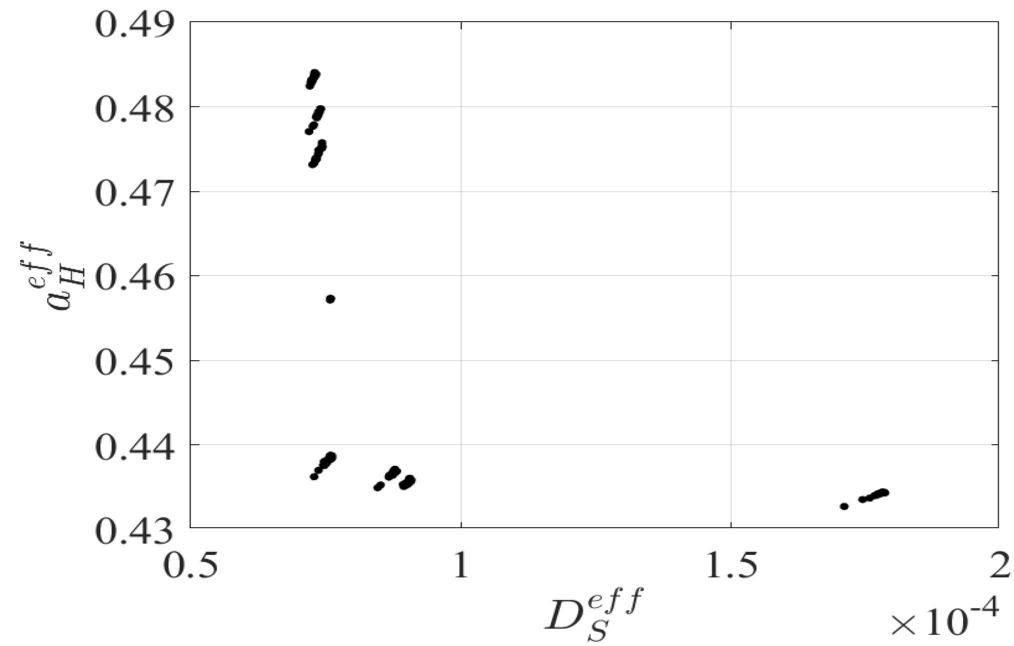

Figure 22: *Robust optimal Pareto front of the mean-effective value of the head acceleration versus suspension deflection*

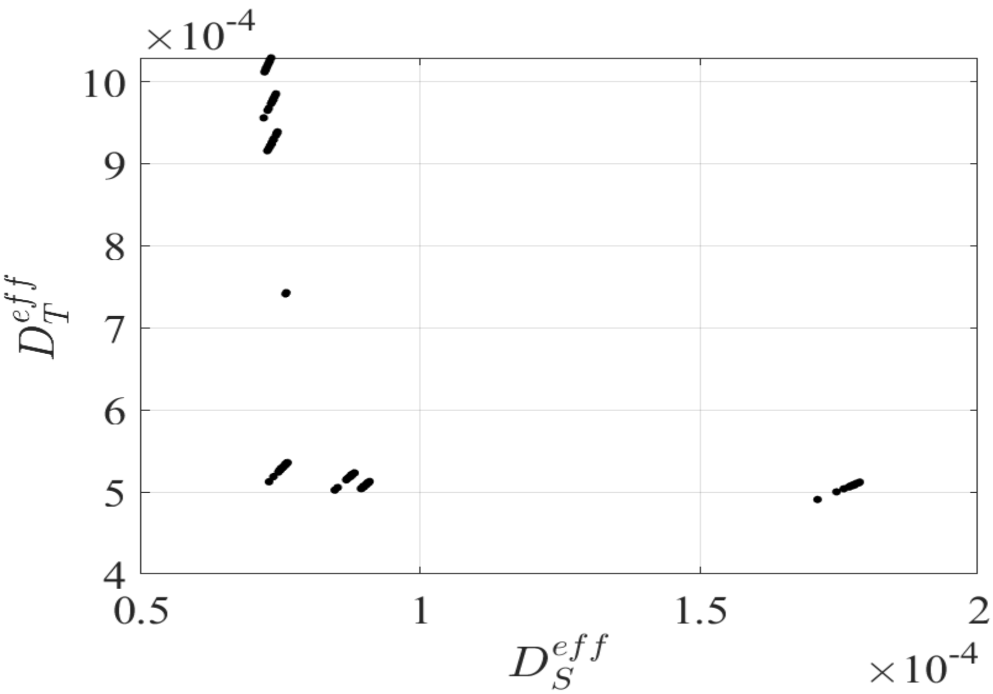

Figure 23: *Robust optimal Pareto front of the mean-effective value tire deflection versus suspension deflection*

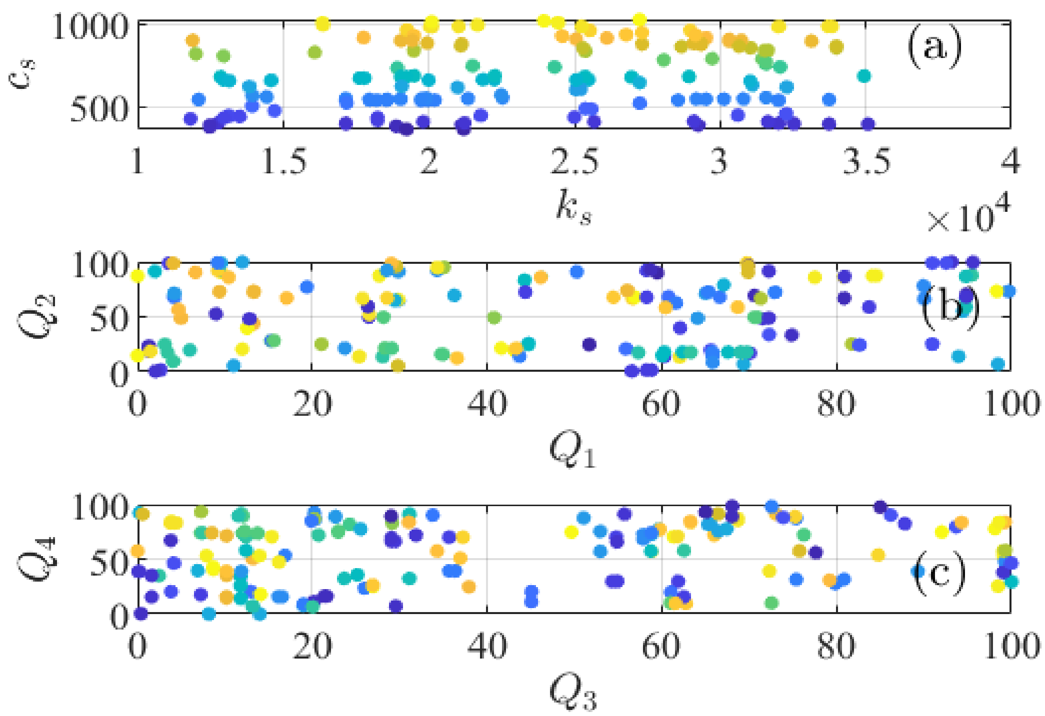

Figure 24: *Robust Pareto Set (a) the color is mapped to the value k_y (b) & (c) the color is mapped to the value of the control weighting factor R.*

The profiles of the suspension deflection at the lower and upper values of $m_s, k_y, k_s, and\ c_s$ are shown in Figures (25) and (26). The responses manifest little deviations from the ideal response (labeled original in the legend). The sprung spring and damping constants seem to have more impact on the S_D profile as compared to the other parameters. Inspecting the profiles of the tire deflection shown in Figures (27) and (28) at different conditions, we notice that the response is insensitive to variations in $m_s, and\ c_s$ and slightly deviate from its ideal profile when $k_y, and\ k_s$ are degraded. Similarly, the passenger head acceleration (see Figures (29) and (30) show little corrupt from its ideal response when the passive elements of the suspension are perturbed. This emphasizes the importance of the robust design of semi-active suspension systems to ensure that the results are less sensitive to the parametric variations and boost the system performance.

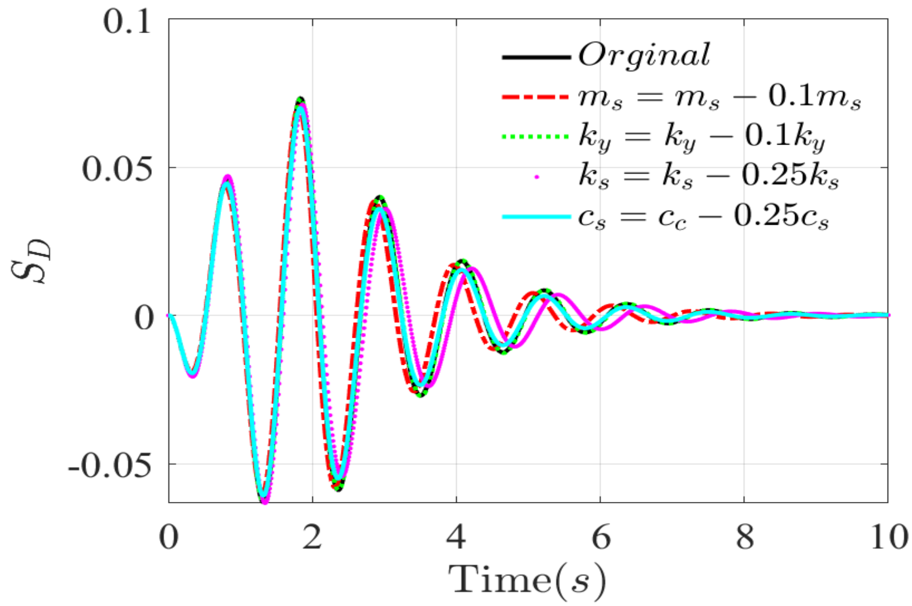

Figure 25: *Time response of suspension deflection at the lower levels of the suspension passive elements.*

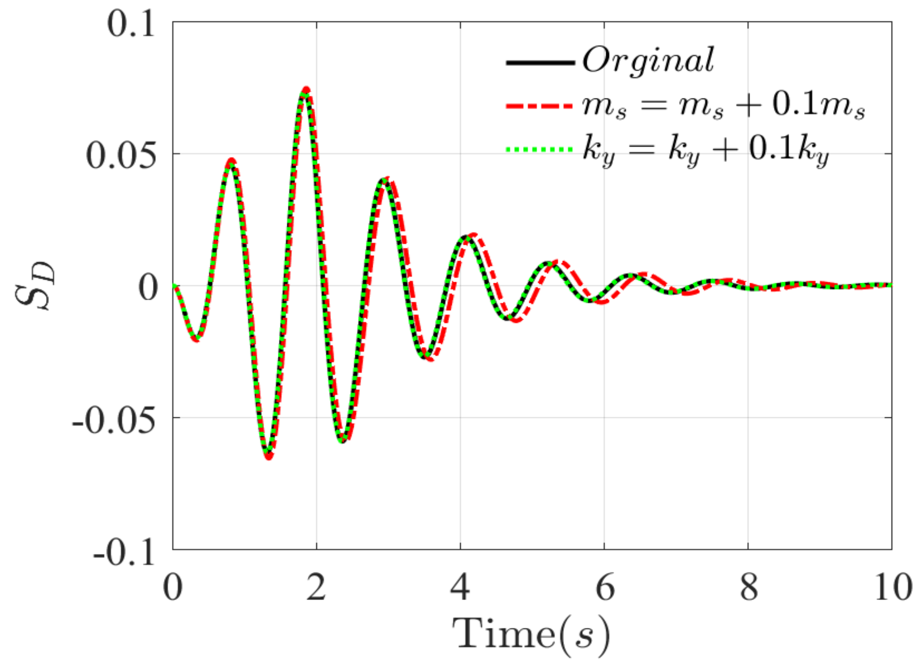

Figure 26: *Time response of suspension deflection at the upper levels of the suspension passive elements.*

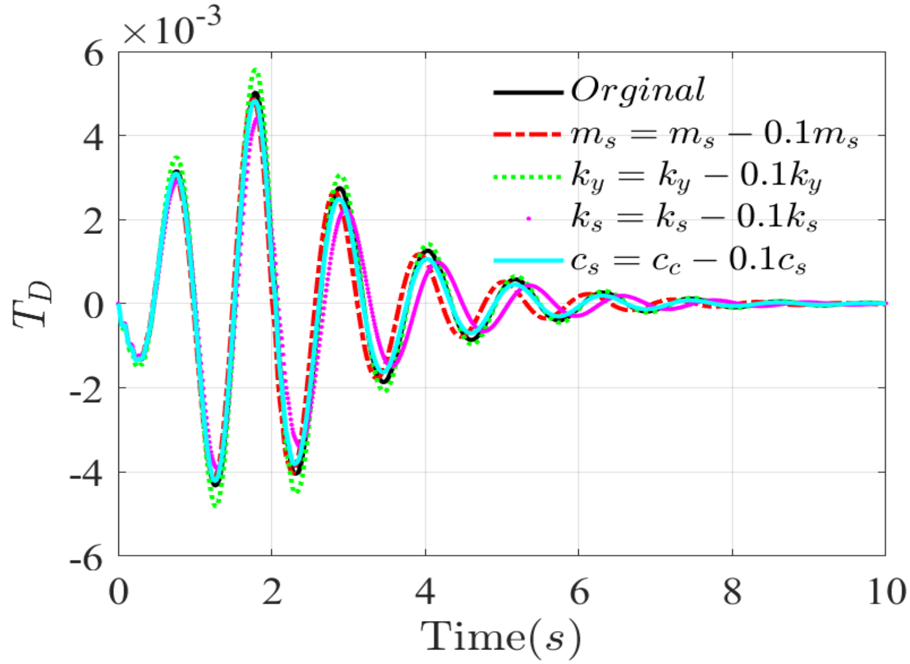

Figure 27: *Time response of tire deflection at the lower levels of the suspension passive elements*

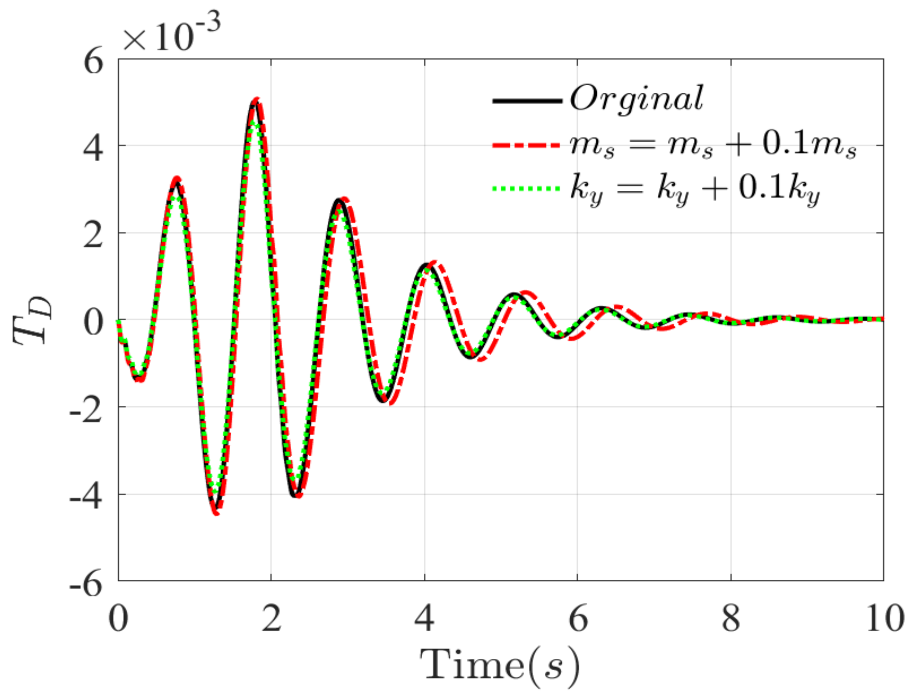

Figure 28: *Time response of tire deflection at the upper levels of the suspension passive elements.*

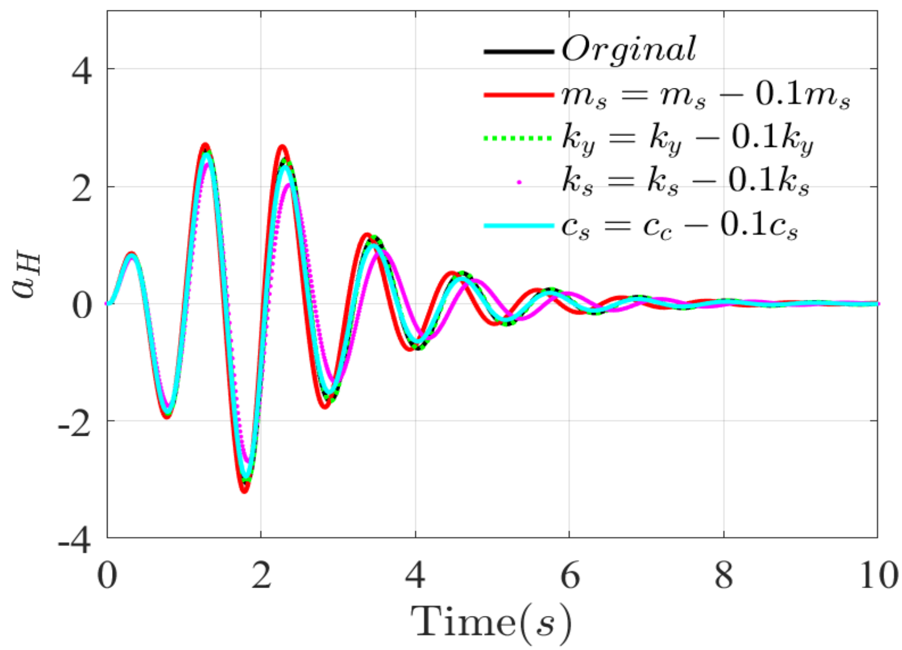

Figure 29: *Time response of head acceleration at the lower levels of the suspension passive passive elements.*

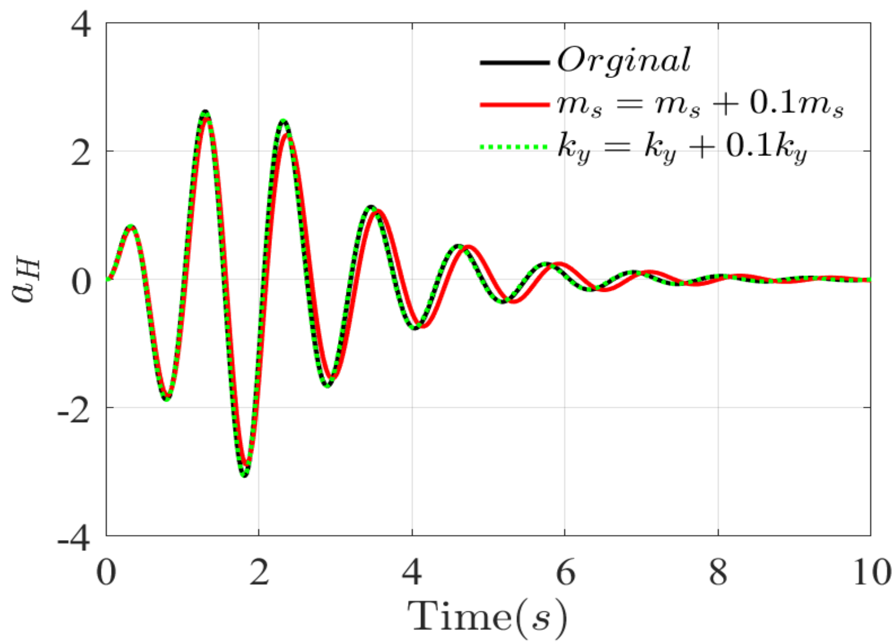

Figure 30: *Time response of head acceleration at the upper levels of the suspension passive elements.*

3.7 Conclusion

We have studied the robust multi-objective design of a semi-active suspension system used in a commercial car. The optimization problem with 8 design parameters and 3 objective functions is solved by the NSGA-II algorithm. The sprung mass of the vehicle, tire stiffness, and suspension stiffness and damping constants are assumed to be uncertain and varied during the optimization to account for their variability. The robust Pareto set, and front are obtained. The Pareto set includes multiple design options from which the decision-maker can choose to implement. Time profiles of the design objectives show that the robust multi-objective design algorithm (RMOA) is effective, guarantees less sensitivity to the suspension passive components and provides with control within the system.

CHAPTER 4: SUMMARY

Robust multi-objective design of a semi-active suspension system and passive suspension system is carried out for a commercial car & racing car. The passive suspension system consisted of pure passive components such as inerters; whereas the semi active suspension system includes active elements that are controlled by a compensator built by linear quadratic regulator (LQR) algorithm. The size of the design parameter space depends on the type of the suspension systems. For passive suspension system, the tire stiffness, inerter's coefficient, and constants of the sprung spring and damper are selected as design parameters. In the case of the semi-active suspension system, the LQR weighting matrices, and coefficients of the tire stiffness, sprung spring, and sprung damper are chosen as decision variables. In both problems, the objectives are the same: minimization of the suspension travel, tire deflection, and passenger' head acceleration. The uncertainty ranges of the passive elements of the suspension systems are defined based on the literature. The robust optimization solutions in terms of Pareto set and front for both systems are obtained by the non- dominating algorithm. Global sensitivity Analysis (GSA) is performed for the semi active suspension system, and the results for sensitivity indices for each individual parameter are obtained. The simulations show that the Pareto front is robust and less sensitive to parametric variations.

Future work will include designing an optimal and robust suspension system for aircraft landing gear, and motorcycles using steering compensators. Furthermore, the idea of robust design of semi-active suspension can be implemented in electric cars and full-car models can be evaluated to justify the success of the methodology.

REFERENCES

A, K. C., N, N., & Begum S, e. a. (2012). Multi-objective Cascade Control of Regulatory Process with Two Conflicting Objectives. *Procedia engineering*, 38: 4057-4063.

A. Baumal, J. M. (1998). Application of genetic algorithms to the design optimization of an active vehicle suspension. *Computer methods in applied mechanics and engineering*, 87-94.

Abdalla, M., Alsharif, M., Atkare, U., Bagwe, R., Boaks, M., Borkar, R., & Brown, D. (2016). DC Motor Drive System Cascade Control Strategy. *Engineering*.

Adhikari, N. P., Choubey, M., & Singh, R. (2012). DC motor control using Ziegler Nichols and genetic algorithm technique. *International Journal of Electrical, Electronics and Computer Engineering 1.1* , 33-36.

aerospaceweb. (2012, 02 24). Retrieved from http://www.aerospaceweb.org/question/aerodynamics/q0167.shtml

Agees Kumar, C., & Kesavan Nair, N. (2012). Multi-objective Cascade Control System Design with an application to Level Control in Liquid Level process. *Life Science Journal, 9*(3).

Alfaro, V. M., Vilanova, R., & Arrieta, O. (2008). Two-degree-of-freedom PI/PID tuning approach for smooth control on cascade control systems. *2008 47th IEEE Conference on Decision and Control*, (pp. 5680-5685).

Alfonso Callejo, J. G. (2015). *Sensitivity-Based, Multi-objective Design of Vehicle Suspension System.* Spain: ASME.

Almutairi, N. B., & Zribi, M. (2010). On the sliding mode control of a ball on a beam system. *Nonlinear dynamics, 59*(1-2), 221.

Anaya-Martinez, M., Lozoya-Santos, J.-d.-J., Félix-Herrán, L., Tudon-Martinez, J.-C., Ramirez-Mendoza, R.-A., & Morales-Menendez, R. (2020). Control of Automotive Semi-Active MR Suspensions for In-Wheel Electric Vehicles. *Journal of applied sciences*, 10.

Basargan, H., Mihάly, A., Gáspár , P., & Sename, O. (2020). Integrated multi-criteria velocity and semi-active suspension control. *2020 28th Mediterranean Conference on Control and Automation (MED).* Saint-Raphaël, France: Institute of Electrical and Electronics Engineers.

Beyer, H. G., & Deb, K. (2001). On self-adaptive features in real-parameter evolutionary algorithms. *IEEE Transactions on evolutionary computation, 5*(3), 250-270.

Bhargav Gadhvi, V. S. (2016). *Multi-Objective Optimization of Vehicle Passive Suspension System using NSGA-II, SPEA2 and PESA-II.* Gandhinagar, India: Science Direct.

Bhavina, R., Jamliya, N., & Vashishta, K. (2013). Cascade control of DC motor with advance controller. *International journal of Industrial Electronics and Electrical Engineering 1.1, 1*(1), 18-20.

Bryson, A. E. (2018). *Applied optimal control: optimization, estimation and control.*. Routledge.

Bulman, D. P. (1997). An experimental and theoretical investigation into the design of an active suspension system for a racing car. *Journal of Automobile Engineering,*, 161-173.

C. C. Papageorgiou, N. E. (2009). Experimental testing and analysis of inerter devices. *Journal of dynamic systems, measurement and control*.

Callejo, A., Jalon, J., Luq, P., & Mantaras, D. (2015). Sensitivity Based Multi-objective Design of Vehicle Suspension Systems. ASME.

Chen, C. (2015). *On the robustness of the linear quadratic regulator via perturbation analysis of the Riccati equation.* Dublin City University: Doctoral dissertation.

Chen, M., Papageorgiou, C., Scheibe, F., & Wan, F.-C. (2009). The missing mechanical circuit element. *IEEE Circuits and Systems Magzine*, 10-26.

Chen, C. Y., Hsu, C. H., Yu, S. H., Yang, C. F., & Huang, H. H. (2009). Cascade PI controller designs for speed control of permanent magnet synchronous motor drive using direct torque approach. *Fourth International Conference on Innovative Computing, Information and Control (ICICIC)* (pp. 938-941). IEEE.

Chen, M., Hu, Y., Huang, L., & Chen, G. (2014). Influence of inerter on natural frequencies of vibration systems. *Journal of Sound and Vibration*, 1874- 1887.

Chen, Y. C., Tu, J. Y., & Wang, F. C. (2015). Earthquake vibration control for buildings with inerter networks. *European Control Conference(ECC)* (pp. 3137- 3142). IEEE.

Chen, Z., Gao, W., Hu, J., & Ye, X. (2010). Closed-loop analysis and cascade control of a nonminimum phase boost converter. *IEEE Transactions on power electronics*, *26*(4), 1237-1252.

Crews, J., Mattson, M. G., & Bucker, G. D. (2011). Multi-objective control optimization for semi-active vehicle suspensions. *Journal of Sound and Vibration*, 5502–5516.

Deb, K. (2001). Multi-objective optimization using evolutionary algorithms. *New York: John Wiley & Sons*, Vol. 16.

Deb, K., & Agrawal, R. B. (1995). Simulated binary crossover for continuous search space. *Complex systems*, *9*(2), 115-148.

Deb, K., & Gupta, H. (2006). Introducing robustness in multi-objective optimization. *Evolutionary computation*, 463- 494.

Deb, K., Pratap, A., Agarwal, S., & Meyarivan, T. A. (2002). A fast and elitist multi-objective genetic algorithm: NSGA-II. *IEEE transactions on evolutionary computation, 6*(2), 182-197.

Derrien, J.-C., & Sécurité, S. D. (2012, September). Electromechanical actuator (EMA) advanced technologies for flight controls. *In International Congress of the Aeronautical Sciences*, 1-10.

Dorf, R. C., & Bishop, R. H. (2011). Modern control systems. Pearson. *Pearson*.

Durillo, J., Nebro, A., Coello, C., Nieto, J., Luna, F., & Alba, E. (2010). A Study of Multi-objective Metaheuristics When Solving Parameter Scalable Problems. *IEEE Transactions on Evolutionary Computation, 14*(4), 618-635.

Durillo, J., Nebro, A., Coello, C., Luna, F., & Alba, E. (2008). A comparative study of the effect of parameter scalability in multi-objective metaheuristics. 1893-1900.

E. Abdellahi, D. M. (2001). Design of active suspension system with model parametric uncertainties. *European Control Conference (ECC)* (pp. 3428–3433). IEE.

El Hajjaji, A., & Ouladsine, M. (2001). Modeling and nonlinear control of magnetic levitation systems. *IEEE Transactions on industrial Electronics, 48*(4), 831-838.

Evangelou, S., Limebeer, D. J., Sharp, R. S., & Smith, M. C. (2007). Mechanical steering compensators for high-performance motorcycles.

Faraj, R., Holnicki-Szulc, J., Knap, L., & Seńko, J. (2016). Adaptive inertial shock-absorber. *Smart Materials and Structures,*, 35-31.

Ferreira, D. V., & Coelho, V. N. (2018). Calibration of a type 2 controller applied to a buck converter: a multi-objective analysis. *Electronic Notes in Discrete Mathematics,* 66, 199-206.

Fossati, G., Miguel, L., & Casas, W. (2019). Multi-objective optimization of the suspension system parameters of a full vehicle model. (pp. 151–177). Springer.

Franklin, G. F., Powell, J. D., Emami-Naeini, A., & Powell, J. D. (1994). Feedback control of dynamic systems. *Reading, MA: Addison-Wesley,* Vol. 3.

Franks, R., & Worley, C. (1956). Quantitative Analysis of Cascade Control. *Ind. and Eng. Chemistry, 48*(6), 1074-1079.

Frej, G., Moreau, X., Hamrouni, E., Benine-Neto, A., & Hernette, V. (2020). A Multi-Modes Semi-Active Suspension Control Strategy for Peugeot 308 RCZ Vehicle. *2020 28th Mediterranean Conference on Control and Automation (MED).* Saint-Raphaël, France: Institute of Electrical and Electronics Engineers.

Fu, H., Pan, L., Xue, Y. L., Sun, L., Li, D. H., Lee, K. Y., & Zheng, S. (2017). Cascaded PI Controller Tuning for Power Plant Superheated Steam Temperature based on Multi-Objective Optimization. *IFAC-PapersOnLine, 50*(1), 3227-3231.

Fu, J., Jean-Charles, M., & Fu, Y. (2017). Modelling and simulation of flight control electromechanical actuators with special focus on model architecting, multidisciplinary effects and power flows. *Chinese Journal of Aeronautics*, 30(1), 47-65.

Gadhvi, B., Savsani, V., & Patel, V. (2016). Multi-objective optimization of vehicle passive suspension system using NSGA-II, SPEA2 and PESA-II. *Procedia Technology*, 361-368.

Gaspari, A. D., Ricci, S., Riccobene, L., & Scotti, A. (2009). Active Aeroelastic Control Over a Multisurface Wing: Modeling and Wind-Tunnel Testing. *AIAA Journal*, 995-2010.

Goga, V., & Kľúčik, M. (2012). Optimization of vehicle suspension parameters with use of evolutionary computation. *Modeling of mechanical and mechatronic systems*. (pp. 174 – 179). Bratislava, Slovakia : ELSEVIER.

Habibi, S., Jeff, R., & Greg, L. (2008). Inner-loop control for electromechanical (EMA) flight surface actuation systems. *Journal of dynamic systems, measurement, and control* , 130(5), 051002. ASME.

Haghighat, S., Martins, J. R., & Liu, H. H. (2012). Aeroservoelastic design optimization of a flexible wing. *Journal of Aircraft*. *49*(2), 432-443.

Hamza, M. F., Yap, H. J., & Choudhury, I. A. (2015). Genetic algorithm and particle swarm optimization based cascade interval type 2 fuzzy PD controller for rotary inverted pendulum system. *Mathematical Problems in Engineering 2015*.

Haupt, R. L., & Ellen Haupt, S. (2004). *Practical genetic algorithms.* John Wiley & Sons,.

Hernández, C., Naranjani, Y., Sardahi, Y., Liang, W., Schütze, O., & Sun, J.-Q. (2013). Simple cell mapping method for multi-objective optimal feedback control design. *International Journal of Dynamics and Control*, 1(3), 231-238.

Homod, R. Z., Sahari, K. S., Mohamed, H. A., & Nagi, F. (2010). Hybrid PID-cascade control for HVAC system. *International journal of systems control,, 1*(4), 170-175.

Hu, X., Huang, Z., & Wang, Z. (2003). Hybridization of the multi-objective evolutionary algorithms and the gradient-based algorithms. *In The 2003 Congress on Evolutionary Computation, 2003. CEC'03*, Vol. 2, pp. 870-877.

Iroz, W. S. (2015). Uncertainties in road vehicle suspensions. *Procedia IUTAM*.

Ismail, M. A., Edward, B., & Holger, S. (2016). Fault detection and classification for flight control electromechanical actuators. *2016 IEEE aerospace conference*, 1-10.

Jamali, A., Shams, H., & Fasihozaman, M. (2014). Pareto multi-objective optimum design of vehicle-suspension system under random road excitations. *Multi body Dynamics*, 282-293.

Jiang, J. Z., Matamoros-Sanchez, A. Z., Goodall, R. M., & Smith, M. C. (2012). Passive suspensions incorporating inerters for railway vehicles. *Vehicle System Dynamics*, 263-276.

Jiang, J. Z., Matamoros-Sanchez, A. Z., Zolotas, A., Goodall, R. M., & Smith, M. C. (2015). Passive suspensions for ride quality improvement of two-axle railway vehicles. *Journal of Rail and Rapid Transit*, 315- 329.

Jones, D. F., Mirrazavi, S. K., & Tamiz, M. (2002). Multi-objective meta-heuristics: An overview of the current state-of-the-art. *European journal of operational research, 137*(1), 1-9.

Kakde, M. R. (2004). Survey on multi-objective evolutionary and real coded genetic algorithms. *In Proceedings of the 8th Asia Pacific symposium on intelligent and evolutionary systems* , (pp. 150-161). Springer.

Kanagarajan, D., Karthikeyan, R., Palanikumar, K., & Paulo Davim, J. (2008). Optimization of electrical discharge machining characteristics of WC/Co composites using non-dominated sorting genetic algorithm (NSGA-II). *International Journal of Advance Manufacturing Technology*, 1124-1132.

Kaya, I., Tan, N., & Atherton, D. P. (2007). Improved cascade control structure for enhanced performance. *Journal of Process Control*, 17(1), 3-16.

Keith, R. D. (2019). *Why f1 rejected proposal to legalise active suspension in 2021*. https://www.racefans.net/2019/07/19/why f1 rejected-proposal-to-legalise-active-suspension-in-2021.

Khadr, A., & Romdhane, L. (2016). Design and optimization of a semi-active suspension system for a two-wheeled vehicle using a full multibody model. *Journal of Multi body dynamics*, 1-17.

Koulocheris, D., Papaioannou, G., & Chrysos, E. (2017). A comparison of optimal semi-active suspension systems regarding vehicle ride comfort. *Materials Science and Engineering.* Athens, Greece: Institute of Physics.

Kumar, C. A., Nair, N., Begum, S., & Tharani, T. (2012). Multi-objective Cascade Control of Regulatory Process with Two Conflicting Objectives. *Procedia engineering, 38*, 4057-4063.

Kumar, V. S., Laura, A. M., Raymond, K., & Jonathan, E. C. (2012). Receptance Based Active Aeroelastic Control Using Multiple Control. *53rd AIAA/ASME/ASCE/AHS/ASC Structures, Structural Dynamics, and Materials Conference.* Honolulu, Hawaii: AIAA Paper.

Kuznetsov, A., Mammadov, M., Sultan, I., & Hajilarov, E. (2011). Optimization of improved suspension system with inerter device of the quartercar model in vibration analysis. *Archive of Applied Mechanics*, 1427- 1437.

Lazaro, J. G., Villegas, H. E., Ruiz, B., & Aldana, A. (2019). Control Design Strategies for Semi-Active Suspension System. *International Mechanical Engineering Congress and Exposition.* Salt Lake City, Utah: American Society of Mechanical Engineers.

Lee, Y., Park, S., & Lee, M. (1998). PID controller tuning to obtain desired closed loop responses for cascade control systems. *Industrial & engineering chemistry research, 37*(5), 1859-1865.

Lehman, A., & Stoilov, V. (2015). Application of the Fourier Amplitude Sensitivity Test (FAST) to Analyze Thermal Performance of Vehicle Underbody Components. *Journal of Materials and Manufacturing*, 6.

Liebeck, R. H. (2004). Design of the Blended Wing Body Subsonic Transport. *Journal of Aircraft*, 10-25.

Loyer, B., & Jézéquel, L. (2009). *Robust design of a passive linear quarter car suspension system using a multi-objective evolutionary algorithm and analytical robustness indexes.* London: Taylor and Francis.

Lucia, D. (2005). The SensorCraft Configurations: A Non-Linear AeroServoElastic Challenge for Aviation. *Proceedings of the 46th AIAA/ASME/ASCE/AHS/ASC Structures, Structural Dynamics and Materials Conference*, (pp. 18-21). Reston, VA.

M. P. Nagarkar, G. J. (2016). Optimization of nonlinear quarter car suspension–seat–driver model. *Journal of advanced research*, 991–1007.

Maffezzoni, C., Schiavoni, N., & Ferretti, G. (1990). Robust design of cascade control. *IEEE Control Systems Magazine, 10*(1), 21-25.

Mahmoud Mohsen, H. K. (2018). Optimal design of passive suspension system of a 6 × 6 multi-wheeled all-terrain vehicle using genetic algorithm.

Mai, V. N., Yoon, D.-S., Choi, S.-B., & Kim, G.-W. (2020). Explicit model predictive control of semi-active suspension systems with magnetorheological dampers subject. *Journal of Intelligent Material Systems*, 1-14.

Majdoub, E. K., Ouadi, H., Belbounaguia, N., Kheddioui, E., Souhail, R., & Ammari1, O. (2018). Optimal Control of Semi-Active Suspension Quarter Car Employing Magnetorheological Damper and Dahl Model. *Renewable Energies, Power Systems &*

Green Inclusive Economy (REPS-GIE). Casablanca, Morocco: Institute of Electrical and Electronics Engineers.

Marler, R. T., & Arora, J. S. (2004). Survey of multi-objective optimization methods for engineering. *Structural and multidisciplinary optimization, 26*(6), 369-395.

McDonough, L. A., Singh, K. V., & Kolonay, R. (2011). Active Control for Coupled Unsteady Aeroelastic Models. *Proceedings of the International Forum on Aeroelasticity and Structural Dynamics (IFASD 2011).* Paris, France.

Mechanical vibration and shock; evaluation of human exposure to whole body vibration in the working enviournment, 1997 part 1 general requirement. Geneva.

Moens, F. (2019). *Design of a generic wing model for basic stall phenomena*. Laval, Canada. HAL.

Nariman-Zadeh, N., Salehpour, M., Jamali, A., & Haghgoo, E. (2010). Pareto optimization of a five-degree of freedom vehicle vibration model using a multi-objective uniform-diversity genetic algorithm (MUGA). Engineering Applications of Artificial Intelligence, 543–551.

Nagarkar, M. P., Patil, G. J., & Patil, R. N. (2016). Optimization of nonlinear quarter car suspension–seat–driver mode*l* (Vol. 7). *Journal of Advanced Research*. Elsevier.

Niahn-Chung Shieha, C. L.-Z. (2004). *Optimal design for passive suspension of a light rail vehicle using constrained multi-objective evolutionary search*.Taiwan: Elsevier.

Nicola, G. D., N. C., & Moglie, M. (2010). *Experimental Investigation and Optimization of a Cascade Cycle*. Purdue.

Ogata, K., & Yang, Y. (2010). Modern control engineering. *Upper Saddle River, NJ: Pearson*, Vol. 17.

Oral, Ö., Çetin, L., & and Uyar, E. (2010). A Novel Method on Selection of Q And R Matrices In The Theory Of Optimal Control. *International Journal of Systems Control, 1*(2).

Papageorgiou, C., Houghton, N., & Smith, M. (2009). Experimental testing and analysis of inerter devices. *dynamic systems, measurement and control*, vol. 131, no. 1.

Pareto, V. (1971). *Manual of political economy*. OXFORD.

Perlikowski, P. B. (2017). Effects of play and inerter nonlinearities on the performance of tuned mass damper. *Nonlinear Dynamics*, 1027 - 1041.

Platanitis, G. W. (2004). Control of a nonlinear wing section using leading-and trailing-edge surfaces. *Journal of Guidance, Control, and Dynamics*, 27(1), 52-58.

Qin, Y., Wang, Z., Yuan, K., & Zhang, Y. (2019). Comprehensive Analysis and Optimization of Dynamic Vibration-Absorbing Structures for Electric Vehicles Driven by In-Wheel Motors. Automation Innovation, 254-262.ResearchGate.

Rathod, B. (2013). Reviews of Cascade Control of Dc Motor with Advance Controller. *International Journal for Scientific Research & Development*, 1121-1123.

Safronov, A. N. (2019). Aviation Meteorology at Several Plane Crash Sites. *Atmosphere*, 10(2), 50.

Sardahi, Y. (2016). Multi-objective optimal design of control systems. *Doctoral dissertation, UC Merced*.

Sardahi, Y., & Boker, A. (2018). Multi-objective optimal design of four-parameter PID controls. *Dynamic Systems and Control Conference. American Society of Mechanical Engineers Digital Collection*. ASME.

Sardahi, Y., & Sun, J.-Q. (2017). Many-objective optimal design of sliding mode controls. *Journal of Dynamic Systems, Measurement, and Control*, 139(1), 014501.

Shibuchi, H., Sakane, Y., Tsukamoto, N., & Nojima, Y. (2009). Evolutionary many-objective optimization by NSGA-II and MOEA/D with large populations. *IEEE International Conference on Systems, Man and Cybernetics*, (pp. 1758-1763).

Shirahatti, A., Prasad, P. S., Panzade, P., & Kulkarni, M. M. (2008). Optimal design of passenger car suspension for ride and road holding. *Journal of the Brazilian Society of Mechanical Sciences and Engineering*, *30*(1), 66-76.

Singh, K. V., & McDonough, L. A. (2014). Optimization of Control Surface Parameters with Augmented Flutter Boundary Constraints. *AIAA Atmospheric Flight Mechanics Conference*, 2014-2050.Atlanta GA.

Singh, K. V., Brown, R. N., & Kolonay, R. (2016). Receptance-based active aeroelastic control with embedded control surfaces having actuator dynamics. *Journal of Aircraft*, *0*, 830-845.

Singh, K. V., McDonough, L. A., Kolonay, R., & Cooper, J. E. (2014). Receptance-based active aeroelastic control using multiple control surfaces. *Journal of Aircraft*, 113-136.

Singh, K. V., McDonough, L. A., Mottershead, J., & Cooper, J. (2010). Active Aeroelastic Control Using the Receptance. *Proceedings of the ASME International Mechanical Engineering Congress and Exposition.* Vancouver, BC, Canada.

Smith, C. A., & Corripio, A. B. (1985). *(1985). Principles and practice of automatic process control* (Vol. 2). New York: Wiley.

Smith, M. (2002). Synthesis of mechanical networks: The inerter. *IEEE Transactions on automatic control*, 1648-1662.

Srinivas, N., & Deb, K. (1994). Muiltiobjective optimization using nondominated sorting in genetic algorithms. *Evolutionary computation*, *2*(3), 221-248.

Takewaki, I., Murakami, S., Yoshitomi, S., & Tsuji, M. (2012). Fundamental mechanism of earthquake response reduction in building structures with inertial dampers. *Structural Control and Health Monitoring*, 590- 608.

Tian, Y., Cheng, R., Zhang, X., & Jin, Y. (2017). PlatEMO: A MATLAB platform for evolutionary multi-objective optimization [educational forum]. *IEEE Computational Intelligence Magazine*, *12*(4), 73-87.

Tunyasrirut, S., & Wangnipparnto, S. (2007). Level control in horizontal tank by fuzzy-pid cascade controller. *World academy of science, engineering and technology*, *25*(1).

Urgoiti, E., Enrique, H., & Iker, G. (2009). Performances of Linear Electro Mechanic Actuators (EMA) for the International Berthing and Docking Mechanism (IBDM). *13th European Space Mechanisms and Tribology Symposium. Vienna*.

Wang, F. C., Hsieh, M. R., & Chen, H. J. (2012). Stability and performance analysis of a full-train system with inerters. *Vehicle System Dynamics*, 545- 571.

Wang, Z., & Behal, A. M. (2012). Continuous robust control for two-dimensional airfoils with leading-and trailing-edge flaps. *Journal of Guidance, Control, and Dynamics*,, 35(2), 510-519.

Wei, X., Jingjing, M., Hongyan, J., & Fei, Y. (2010). The main steam temperature cascade control of high order differential of feedback controller. *In 2010 International Conference on Intelligent System Design and Engineering Application, IEEE, 2*, pp. 683-687.

Woźniak, P. (2010). Multi-objective control systems design with criteria reduction. *In Asia-Pacific Conference on Simulated Evolution and Learning*, 583-587.

Wu, J., Zhou, H., Liu, Z., & Gu, M. (2020). Ride Comfort Optimization via Speed Planning and Preview Semi-Active Suspension Control for Autonomous Vehicles on Uneven Roads. *IEEE Transactions on Vehicular Technology*, 8343 - 8355.

Wu, X., Wei, X., & Guo, W. (2012). Multi-objective ecological operation model of cascade hydropower reservoirs. *Procedia Engineering*, 29, 3996-4001.

Xiaolong, W. (2017). Semi-active adaptive optimal control of vehicle suspension with a magnetorheological damper based on policy iteration. *Journal of Intelligent Material Systems and Structures*, 255-264.

Xu, X ., Sardahi, Y., & Zheng, C. (2018). Multi-Objective Optimal Design of Passive Suspension System With Inerter Damper. *In ASME 2018 Dynamic Systems and Control Conference. American Society of Mechanical Engineers Digital Collection.*

Ye, H., & Zheng, L. (2019). Comparative study of semi-active suspension based on LQR control and H2/H∞ multi-objective control. *Chinese Automation Congress (CAC).* Hangzhou: Institute of Electrical and Electronics Engineers.

Yokozeki, T., Sugiura, A., & Hirano, Y. (2014). Development of variable camber morphing airfoil using corrugated structure. *Journal of Aircraft*, 51(3), 1023-1029.

Zhao, Y. (2009). Flutter suppression of a high aspect-ratio wing with multiple control surfaces. *Journal of Sound and Vibration*, 490-513.

APPENDIX A: INSITITUTIONAL REVIEW BOARD LETTER

MARSHALL UNIVERSITY
www.marshall.edu

Office of Research Integrity

November 10, 2020

Muhammad Ali Khan
1423 Commerce Avenue, Apt 15
Huntington, WV 25701

Dear Mr. Khan:

This letter is in response to the submitted thesis abstract entitled *"Robust Multi-Objective Design of Suspension Systems."* After assessing the abstract, it has been deemed not to be human subject research and therefore exempt from oversight of the Marshall University Institutional Review Board (IRB). The Code of Federal Regulations (45CFR46) has set forth the criteria utilized in making this determination. Since the information in this study does not involve human subjects as defined in the above referenced instruction, it is not considered human subject research. If there are any changes to the abstract you provided then you would need to resubmit that information to the Office of Research Integrity for review and a determination.

I appreciate your willingness to submit the abstract for determination. Please feel free to contact the Office of Research Integrity if you have any questions regarding future protocols that may require IRB review.

Sincerely,

Bruce F. Day

Bruce F. Day, ThD, CIP
Director

WE ARE... MARSHALL.

One John Marshall Drive • Huntington, West Virginia 25755 • Tel 304/696-4303
A State University of West Virginia • An Affirmative Action/Equal Opportunity Employer

APPENDIX B: RACING CAR MODEL

```
function dx= RacingCarModel(t,x,TunePars)

%% Tunable Parameters

% ky=233 KN/m ks=300KN/m cs=8000 B=4

% TunePars= [10.0e3 5.0e3 200 50].

ky=TunePars (1); ks=TunePars (2); cs=TunePars (3);

B=TunePars(4);

%% System Paramters

m=65;

mt= (2*m)/7;

mp=(5*m)/7;

mu= 23; % it is about 8.5 kg without the wheel rim

ms=180; % The weight of racing is between 702-734 kg

ct=1360.

kt=45005.3.

kc=1000;

cc=90;

Ms=[mt 0 0 0;0 mp 0 0;0 0 ms+B -B; 0 0 -B mu+B];

Cs=[-ct ct 0 0;ct -ct-cc cc 0;0 cc -cc-cs cs;0 0 cs -cs];
```

```
% Ks= [kt -kt 0 0;kt-kc kt kc 0;0 -kc kc-ks ks; 0 0 ks ks+ky]*(-1);

Ks= [-kt kt 0 0;kt -kt-kc kc 0;0 kc -kc-ks ks; 0 0 ks -ks-ky];%  Bs= [0 0 0 ky]'.

%% State-Space Model

A= [zeros (4) eye(4); Ms\Ks Ms\Cs];

Ba=[zeros (4,1); Ms\Bs].

%% State-Space Equation

dx=A*x+Ba*zr.
```

APPENDIX C: UNCERTAINTY RANGES FOR PASSIVE SUSPENSION SYSTEM

```
rng (advance)
uncertainities = [0.1 0.05 .08 0.03]; % uncertianities in the design parameters samps=20;
CostFunction=@(TunePars)
Supension_inerter_Objectives_Robust_V2(TunePars,uncertainities,samps);
% CostFunction=@(TunePars)Solver_SuspensionSystemObjs (TunePars);
% ky=TunePars(1); % Tire Stiffness
% ks=TunePars(2);% Sprung-Mass Stiffness
% cs=TunePars(3);% Sprung-Mass damper
% B=TunePars(4);% inerter coefficient.
%   ky  ks cs  B
%   180e3 <ky<240e3
%   10e3 <ks<25e3
%   2e3 <cs<4e3
%   0 <B<4
ub =[240e3  25e3 4e3  4];
gens = 50*length(lb);
obj=3;
%    TunePars=[200.0e3 15.0e3 1000 2];
save(filename);
```

```
R_HA=Objs(:,1);

R_CF=Objs(:,2);

R_TD =Objs(:,3);

R_SD=Objs(:,4);

%Obj=[R_HA,CF,TD,SD];

plot(R_HA,R_SD, *)


ky=TunePars          (:,1);

ks=TunePars          (:,2);

cs=TunePars          (:,3);

B=TunePars          (:,4);
```

APPENDIX D: SEMI-ACTIVE SUSPENSION SYSTEM PARAMETERS

```
function dx=CommercialCarModel(t,x,TunePars)
%% bold Parameters
% ks in [11750,35250]
%cs in [350,1050]
% ky in [95000,285000]
ky=TunePars(1);  ks=TunePars(2);  cs=TunePars(3);
%% LQR
R=TunePars(4);
Q=zeros (4).
Q (1,1) =TunePars(5); Q(2,2)=TunePars(6);
Q (3,3) =TunePars(7); Q(4,4)=TunePars(8);
%% System Paramters
m=65; % checked
mt= (2*m)/7; % checked
mp=(5*m)/7; % checked
mu= 40; % it is about 8.5 kg without the wheel rim
ms=290; % Ref: 2016-Optimization of nonlinear quarter car suspension–seat–driver model
ct=1360; % checked
kt=45005.3; % checked
```

```
kc=10000

cc=900; %

%% System matrices Active

Ms=[mt 0 0 0;0 mp 0 0;0 0 ms 0; 0 0 0 mu];% checked

Cs=[-ct ct 0 0;ct -ct-cc cc 0;0 cc -cc-cs cs;0 0 cs -cs];

% Cs=[ct -ct 0 0;-ct ct+cc -cc 0;0 -cc cc+cs -cs;0 0 -cs cs]*(-1);

% Ks=[kt -kt 0 0; kt-kc kt kc 0; 0 -kc kc-ks ks; 0 0 ks ks+ky]*(-1);

Ks=[-kt kt 0 0;kt -kt-kc kc 0;0 kc -kc-ks ks; 0 0 ks -ks-ky];% checked

Bzy=[0 0 0 ky]';% checked

But=[0 0 1 -1]'; % checked
```

APPENDIX E: LINEAR QUADRATIC CONTROLLER

```
%% State-Space Model
A=[zeros(4) eye(4);Ms\Ks Ms\Cs];% checked Bd=[zeros(4,1);Ms\Bzy];%
Bu=[zeros(4,1);Ms\But];%
%% Control Design
AZsZu=[0, 0, 1, 0;0 , 0, 0, 1;...
-ks/ms, ks/ms, -cs/ms, cs/ms;...
ks/mu, -(ks/mu+ky/mu), cs/mu, -cs/mu];
BZsZu=[0,0, 1/ms, -1/mu]';
K=lqr(AZsZu,BZsZu,Q,R);
u=(K(1)*x(3)+K(2)*x(4)+K(3)*x(7)+K(4)*x(8));
% open loop
dx=A*x+Bd*zy+Bu*u;
```

APPENDIX F: DEFINING NOISE PARAMETERS FOR GSA

```
addpath('StrongSystem').

for opt=1:3

% create a new project

set = set_Create();

%%  adding Parameters

% Nominal Values

m=65.

mt= (2*m)/7.

mp=(5*m)/7.

ms=290.

ct=1360.

kt=45005.3.

cc=900;

kc=10000;

NoiseP=[   mt   mp  ms    ct  kt    cc   kc];

%NoiseP= [0.2  0.2   0.1  0.2  0.2   0     0];

up=NoiseP. *un_ub_KP+NoiseP ;

% Set the number of samples for the quasi-random Monte Carlo

sampling set.N = 1000;
```

% Initialize the project by calculating the model at the sample points

% set = Add Input (set, @ () pdf_Uniform (up (1)), parameter1)

% set = Add Input (set, @ () pdf_Uniform (up (2)), parameter2)

% set = Add Input (set, @ () pdf_Uniform (up (3)), parameter3)

% set = Add Input (set, @ () pdf_Uniform (up (4)), parameter4)

% set = Add Input (set, @ () pdf_Uniform (up (5)), parameter5)

% set = Add Input (set, @ () pdf_Uniform (up (6)), parameter6)

% set = Add Input (set, @ () pdf_Uniform (up (7)), parameter7)

pro = GSA_Init(set);

%Calculate the first order global sensitivity coefficients by using FAST Sfast

= GSA_FAST_GetSi(set);

APPENDIX G: FOURIER COEFFICIENTS CALCULATION

```
function Si = GSA_FAST_GetSi(set)

% retrieve the number of input variables

k = length(pro.Inputs);

% set the number of discrete intervals for numerical integration of (13)

MAXHEIGHT = 6.2’

% increasing this parameter makes more precise the numerical integration

M = 11;

% read the table of incommensurate frequencies for k variables

W = _FAST_GETFreqs(k);

% set the maximum integer frequency

Wmax = W(k).

% calculate the Nyquist frequency and multiply it for the number of

% intervals

K = 2*M*Wmax+1;

q = (AS-1)/2;

% integration

K1 = pi/2*(2*(1:AS)-AS-1)/AS;

alpha = W'*K1
```